ELSEVIER

Contents lists available at ScienceDirect

Ceramics International

journal homepage: www.elsevier.com/locate/ceramint





Antimicrobial properties of co-doped tricalcium phosphates $Ca_{3-2x}(M'M'')_x(PO_4)_2$ (M = Zn^{2+} , Cu^{2+} , Mn^{2+} and Sr^{2+})

Dina V. Deyneko ^{a,b,*}, Inna V. Fadeeva ^c, Elena Yu Borovikova ^{d,e}, Pavel B. Dzhevakov ^a, Pavel V. Slukin ^f, Yufeng Zheng ^g, Dandan Xia ^h, Bogdan I. Lazoryak ^a, Julietta V. Rau ^{i,j}

- ^a Department of Chemistry, Lomonosov Moscow State University, 119991, Leninskie Gory, 1, Moscow, Russia
- b Laboratory of Arctic Mineralogy and Material Sciences, Kola Science Centre, Russian Academy of Sciences, 184209, 14 Fersman str., Apatity, Russia
- A.A. Baikov Institute of Metallurgy and Material Science, Russian Academy of Sciences, 119334 Leninsky Prospect 49, Moscow, Russia
- ^d Geology Department, Lomonosov Moscow State University, 119991, Leninskie gory, 1, Moscow, Russia
- ^e Laboratory of Nature-Inspired Technologies and Environmental Safety of the Arctic, Kola Science Centre, Russian Academy of Sciences, 184209, 14 Fersman str, Apatity, Russia
- f State Research Center for Applied Microbiology and Biotechnology, Obolensk, Moscow Region, 142279, Russia
- g School of Materials Science and Engineering, Peking University, No.5 Yi-He-Yuan Road, Hai-Dian District, 100871, Beijing, China
- ^h Department of Dental Materials, Peking University School and Hospital of Stomatology, Beijing, 100081, China
- i Istituto di Struttura della Materia, Consiglio Nazionale delle Ricerche (ISM-CNR), Via del Fosso del Cavaliere, 100 00133 Rome, Italy
- ^j I.M. Sechenov First Moscow State Medical University, Institute of Pharmacy, Department of Analytical, Physical and Colloid Chemistry, Trubetskaya 8, Build. 2, 119991, Moscow, Russia

ARTICLE INFO

Keywords:
Substituted tricalcium phosphate
Doped tricalcium phosphate
Co-doped TCP
TCP structure
Antimicrobial activity
Zn
Cu

Mn Sr

ABSTRACT

The substituted (Ca^{2+}/Cu^{2+}) , and co-substituted (Cu^{2+}/Zn^{2+}) , (Cu^{2+}/Sr^{2+}) , and (Sr^{2+}/Mn^{2+}) β-tricalcium phosphate $(\beta\text{-TCP})$ -based $Ca_{3\cdot2x}(M'M'')_x(PO_4)_2$ $(M=Zn^{2+},Cu^{2+},Mn^{2+})$ and Sr^{2+} solid solutions have been synthesized using solid-state route. The powder X-ray diffraction study shows the formation of β-TCP-type structure as the main phase in all solid solutions. The crystal structures and chemical compositions were approved using Fourier-transform infrared (FT-IR) absorption spectra and energy-dispersive X-ray spectrometry (EDX) data, respectively. The unit cell parameters and volume of as-synthesized samples directly depend on the radius of the incorporated ions. The limits of the single-phase solid solutions were found based on the possible occupation of the crystal sites in β-TCP structure. For the divalent ions with small radii, such as Cu^{2+} or Zn^{2+} , the limit composition was found as Zn^{2-1} Zn^{2+} and Zn^{2+} . The enlargement of the unit cell by incorporation of Zn^{2+} and Zn^{2+} and Zn^{2+} . The enlargement of Zn^{2+} or Zn^{2+} or Zn^{2+} and Zn^{2+} . The antibacterial properties were studied on 4 bacteria (Zn^{2+} and Zn^{2+}). The antibacterial properties were studied on 4 bacteria (Zn^{2+} and Zn^{2+}

1. Introduction

Among phosphates which can be used in the modern tissue engineering whitlockite-based materials $(Ca_{18}Mg_2(HPO_4)_2(PO_4)_{12})$ [1] are of great importance due to their higher stability in acidic environment, better osteogenic activity, higher resorbability [2], etc., than other phosphates, such as hydroxyapatite $Ca_{10}(PO_4)_6(OH)_2$ (HAP) or brushite $(CaHPO_4 \cdot 2H_2O)$. Natural mineral whitlockite and synthetic β - $Ca_3(PO_4)_2$

(β-TCP) are isostructural and have very similar properties. The hydrogen-containing whitlockite-type compounds can be synthesized only under the pressure in the autoclaves [3]. The difficult synthetic route of whitlockite-type phases limits their application in medicine. At the same time β -Ca₃(PO₄)₂ can be simply obtained both by solid-phase [4,5] and precipitation from solution [6] methods. In addition, various mono-, di-, and trivalent ions can be doped into the β -TCP without significant distortion of the structure. The incorporation of

^{*} Corresponding author.. Chemistry Department, Moscow State University, Leninskie Gory 1, 119991, Moscow, Russia. *E-mail address:* deynekomsu@gmail.com (D.V. Deyneko).

small (Mg²⁺, Zn²⁺, Cu²⁺) and large (Sr²⁺, Ba²⁺) divalent ions into the β-Ca₃(PO₄)₂ structure is of great biological interest. The presence of such ions in the β-TCP host noticeably changes the functional properties. Strontium has a beneficial effect on bone regeneration [7], Zn²⁺ affects on the antibacterial properties, resorbing activity of mature osteoclasts [8], and bone mineral formation. Currently, lots of studies are devoted to the substitution of Ca^{2+} in the initial β -TCP host by mono-, di-, and trivalent ions [4,9-13] in order to achieve new biologically active materials with outstanding functional properties. Co-substitutions strategy in the β -TCP host is expected to offer the combined advantages provided by the presence of two (or more) ions in the structure. Co-doping in the β-TCP can combine various effects, such as, antibacterial and anti-inflammatory activities with stimulation of bone cells in Zn²⁺/Ag⁺ pair [14], osteoclastogenesis and osteoclastic resorption [15] in Sr^{2+}/Mg^{2+} pair, for instance. The previously studied co-doped β -TCP compounds are listed in Table 1.

There is a large number of studies on the di- and trivalent ions substitutions in the β-TCP host and bioactive properties of these solid solutions. The summarized data on the co-doping ions in the β-TCP structure are shown in Table 1. We also provided calculated formulas from the literature experimental selection formulas, and the observed chemical compositions obtained by given energy-dispersive X-ray analysis (EDX) or inductively coupled plasma - optical emission spectrometry (ICP-OES) data in Table 1. It can be seen from the available data that there is no universal choice in concentration of doping ions, moreover, different methods are applied to biological studies. So, it is rather difficult to compare the properties of the different compounds. Furthermore, the studies of such substitutions are not always carried out, taking into account the crystal chemical consideration of the β-TCP structure and the maximum structure capacity to the substitutions of various divalent ions. Most often, researchers overestimate the possible limits of calcium substitution for other cations in the $\beta\text{-TCP}$ structure (Table 1). The limits of Ca²⁺ substitution by Zn²⁺, Cu²⁺, Mn²⁺, and Sr²⁺ using crystal chemistry and previously published data are substantiated in the Discussion. We also provide our comments on the limit compositions of solid solutions and the expected phase composition along with the analysis of the reference data on the properties of substituted tricalcium phosphates (Table 1).

To the best of our knowledge, there are no studies on co-doping Cu^{2+}/Zn^{2+} or Sr^{2+}/Mn^{2+} in the β -TCP structure. Also, there were no yet provided antimicrobial activity study on Cu^{2+}/Sr^{2+} co-doping β -TCP. The comparative data on the effect of Ca^{2+}/Cu^{2+} , Cu^{2+}/Zn^{2+} , Cu^{2+}/Sr^{2+} , and Sr^{2+}/Mn^{2+} co-doping ions on the bioactive properties of solid solutions with the β -TCP structure are presented in this work for the first time.

2. Experimental

2.1. Sample preparation

To evaluate the antimicrobial activity of different compositions the following substituted and co-substituted samples were prepared: $\beta\text{-TCP}(1),\,\beta\text{-TCP-Cu}(2),\,\beta\text{-TCP-Cu}+Zn$ (3), $\beta\text{-TCP-Cu}+Sr$ (4) and $\beta\text{-TCP-Mn}+Sr$ (5) (Table 2). The samples (1)–(5) (Table 2) were synthesized using a high temperature solid-state reaction. The initial reagents of «analytical grade » purity were used: CaO freshly calcined at 900 °C, Cu(NO₃)₂, Mn(NO₃)₂, Zn(NO₃)₂, Sr(NO₃)₂ and (NH₄)₂HPO₄ purchased from Sigma-Aldrich. The quantities of the initial reagents were calculated according to equations (1)–(3).

$$3\text{CaO} + 2(\text{NH}_4)_2\text{HPO}_4 \rightarrow \text{Ca}_3(\text{PO}_4)_2 + 4\text{NH}_3 + 3\text{H}_2\text{O}$$
 (1)

 $2.5CaO + 0.5Cu(NO_3)_2 + 2(NH_4)_2HPO_4 \rightarrow$

$$Ca_{2.5}Cu_{0.5}(PO_4)_2 + 3.6NH_3 + 3.9NO_2 + 3.2H_2O$$
 (2)

$$2.8\text{CaO} + 0.1 \text{ M(NO}_3)_2 + 0.1 \text{ M'(NO}_3)_2 + 2(\text{NH}_4)_2 \text{HPO}_4 \rightarrow$$

$$Ca_{2,8}M_{0,1}M'_{0,1}(PO_4)_2 + 4NH_3\uparrow + 0.4NO_2\uparrow + 3H_2O\uparrow$$
 (3)

Where $M - Cu^{2+}$ or Mn^{2+} , and $M' - Zn^{2+}$; Sr^{2+} .

After sintering, the samples (1)–(5) were calcinated at 1200 $^{\circ}$ C (the duration of the heat treatment was 4 h).

2.2. Experimental description

Powder X-ray diffraction (PXRD) data were collected on a Thermo ARL X'TRA powder diffractometer (Bragg-Brentano geometry, Scintillator detector, CuK α radiation, $\lambda = 1.5418$ Å, Thermo Fisher Scientific, Waltham MA, USA). PXRD data were collected at room temperature over 20 range between 5° and 65° with a step interval of 0.02°. The phase analysis was performed applying Crystallographica Search-March program (version 2.0.3.1) and JCPDS PDF-2 database. The quantitative phase analysis was done by means of the Rietveld method and JANA2006 software [30]. Crystallographic data, including the space group (SG) and unit cell parameters, were used as initial parameters along with the atomic coordinates of β-Ca₃(PO₄)₂, Ca₃Cu₃(PO₄)₄, Zn₃(PO₄)₂ and Ca₂P₂O₇. The background was refined with a fifteenth-order polynomial. The peak profile was refined by a modified Pseudo-Voigt function. The unit cell parameters were refined, whereas the atomic coordinates were not. After the last refinement, a good agreement was observed between the experimentally obtained and the calculated PXRD patterns.

The Fourier-transform infrared (FT-IR) absorption spectra of the synthesized compounds in middle IR were obtained on FSM 1201 FTIR spectrometer in the wavenumber region 4000–400 $\rm cm^{-1}$ with the spectral resolution better than 2 $\rm cm^{-1}$ using a standard KBr disk technique. The IR attenuated total reflection (ATR) spectra in the farinfrared region were registered using Bruker IFS 125HR Fourier spectrometer with ATR module. A powdered sample was put on a diamond crystal of ATR module, and then pressed it. The spectral resolution was 2 $\rm cm^{-1}$.

Scanning electron microscopy (SEM) observations were performed using a Tescan VEGA3 scanning electron microscope equipped with an Oxford Instruments X-Max 50 silicon drift energy-dispersive X-ray spectrometry (EDXs) system with AZtec and INCA software. Samples were coated with a thin layer of carbon for SEM examinations. SEM images were acquired using secondary electron (SE) imaging and backscattered electron (BSE) imaging technique. The local cation composition of disk fragments was determined by SEM-EDX. The EDX analysis results were based on the MgK, ZnK, SrK, MnK, CaK and PK edge lines. The oxygen content was not quantified by EDX.

Antibacterial activities of all as-synthesized samples (1)–(5) (Table 2) were examined. To evaluate the antimicrobial activity the samples were autoclaved at 121 °C for 20 min at a pressure of 1.1 bar. The powder was diluted 1:1000 (w/v) in BHI broth (Brain Heart Infusion, DIFCO, Sparks, USA). The effect of each compound was evaluated towards the growth of 5 different microorganisms 4 bacteria (*S. aureus, P. aeruginosa, E. coli and E. faecalis*) and 1 fungus (*C. albicans*). The experiment was performed by growing the microorganisms in the presence of the different compounds, in slow stirring, the bacteria at 37 °C, while the fungus at 24 °C. After 24 h, the growth of the microorganisms was evaluated by reading with a Biophotometer D30 (Eppendorf, Hamburg, Germany) the OD600nm of the microorganism growth medium. The experiment was carried out in triplicate and the results are expressed as the mean \pm standard deviation (SD).

3. Results and discussion

3.1. PXRD study

Fig. 1 shows parts of PXRD patterns of the as-prepared (1)–(5) samples. The analysis of the data is presented in Table 2. According to

 Table 1

 Co-doped with different ions β-TCP structures and calculated expected and observed formula along with features of the crystal structure and physical or biological properties.

Doping ions	%, substitution	Calculated Expected formula The limit compositions were calculated by us using crystallochemical and literature data on the limits of substitution of calcium for other cations	Formula from the data (EDX or ICP-OS)	Crystal structure features. Our comments are in italics font. x, y – concentration of the host or dopant ions, respectively, in $Ca_xM_y(PO_4)_2$	Physical or biological enhancement by doping ions	Ref
Sr ²⁺ / Zn ²⁺	From Sr ²⁺ :Zn ²⁺ (1.20:1.20) mol% to Sr ²⁺ :Zn ²⁺ (4.8:4.8) mol%	$\begin{array}{l} \text{Ca}_{2.688}\text{Sr}_{0.156}\text{Zn}_{0.156}(\text{PO}_4)_2\\ \text{Ca}_{1.752}\text{Sr}_{0.624}\text{Zn}_{0.624}(\text{PO}_4)_2\\ \text{For some compositions, the substitution limit for}\\ \text{Zn is violated. The limiting composition is}\\ \text{described by the formula}\\ \text{Ca}_{0.428}\text{Sr}_{2.286}\text{Zn}_{0.286}(\text{PO}_4)_2 \end{array}$	$\begin{array}{l} Ca_{2.693}Sr_{0.153}Zn_{0.154}(PO_4)_2 \\ Ca_{1.756}Sr_{0.625}Zn_{0.619}(PO_4)_2 \end{array}$	Decreasing of the unit cell parameters. Preferentially occupation in M4 (Sr^{2+}) and M5 (Zn^{2+}) sites from the Rietveld refinement. Compositions with $x(Ca) < 2.571$ and $y < (Zn^{2+}) > 0.286$ (2.2 mol.%) must contain impurity phase	The thermal stability of β -TCP was significantly improved by co-doping. Co-substituted β -TCP did not display better mineralization ability than pure β -TCP.	[16]
Sr ²⁺ / Zn ²⁺	1.0 wt% Sr ²⁺ +0.25 wt% Zn ²⁺	$Ca_{2.723}Sr_{0.037}Zn_{0.24}(PO_4)_2$ The limiting composition is not violated. The limiting composition is described by the formula $Ca_{0.428}Sr_{2.286}Zn_{0.286}(PO_4)_2$	Not provided	Decreasing of the unit cell parameters. substitution results in the higher density. The composition expected to be single-phase.	Co-doping influences on the grain size of the crystallites and the samples have higher crystallinity. Insignificant effect on initial cell attachment was detected. However, the formation of osteoclast-like-cells was noticed after 8 days of culture on all co-doped β-TCP substrates.	[17]
Sr ²⁺ / Mg ²⁺	From Sr ²⁺ :Mg ²⁺ (2.00:2.00) mol% to Sr ²⁺ :Mg ²⁺ (4.00:4.00) mol%	$Ca_{2.88}Sr_{0.06}Mg_{0.06}(PO_4)_2$ $Ca_{2.76}Sr_{0.12}Mg_{0.12}(PO_4)_2$ The limiting composition is not violated. The limiting composition is described by the formula $Ca_{0.428}Sr_{2.286}Mg_{0.286}(PO_4)_2$	$\begin{array}{l} Ca_{2.86}Sr_{0.06}Mg_{0.08}(PO_4)_2 \\ Ca_{2.77}Sr_{0.11}Mg_{0.12}(PO_4)_2 \end{array}$	Decreasing of the unit cell parameters. The co-doped compositions expected to be single-phase.	Co-doping increases the $\beta{\to}\alpha{\text{-TCP}}$ transition temperature. The samples have higher densification rate. The reduction of the grain sizes as well as the more homogenous grain size distributions was detected.	[18]
Sr ²⁺ / Cu ²⁺	From Sr ²⁺ :Cu ²⁺ (0.63:0.63) mol% to Sr ²⁺ :Cu ²⁺ (2.52:2.52) mol%	$Ca_{2.836}Sr_{0.082}Cu_{0.082}(PO_4)_2$ $Ca_{2.345}Sr_{0.328}Cu_{0.328}(PO_4)_2$ For some compositions, the substitution limit for Cu is violated. The limiting composition is described by the formula $Ca_{0.428}Sr_{2.286}Cu_{0.286}(PO_4)_2$	Ca _{2.844} Sr _{0.077} Cu _{0.079} (PO ₄) ₂ Ca _{2.337} Sr _{0.329} Cu _{0.334} (PO ₄) ₂	Decreasing of the unit cell parameters. Preferentially occupation in M4 (Sr^{2+}) and M5 (Cu^{2+}) sites from the Rietveld refinement. Compositions with $x(Ca) < 2.571$ and $y (Cu^{2+}) > 0.286$ (2.2 mol.%) must contain impurity phase.	The deposition of the co-doped samples on the titanium alloy and heating up to $1000^{\circ}\mathrm{C}$ resulted in no phase changes and the uniform deposition in the coating confirmed by the Rietveld refinement.	[19]
Mg ²⁺ / Cu ²⁺	From Mg ²⁺ /Cu ²⁺ (0.63:0.63) mol% to Mg ²⁺ /Cu ²⁺ (2.52:2.52) mol%	$\begin{array}{l} Ca_{2.836}Mg_{0.082}Cu_{0.082}(PO_4)_2\\ Ca_{2.345}Mg_{0.328}Cu_{0.328}(PO_4)_2\\ For some compositions, the substitution limit for\\ (Cu^{2+}+Mg^{2+}) is violated. The limiting\\ composition is described by the formula\\ Ca_{2.714}(Mg,Cu)_{0.286}(PO_4)_2 \end{array}$	$\begin{array}{l} \text{Ca}_{2.84}\text{Mg}_{0.085}\text{Cu}_{0.075}(\text{PO}_4)_2 \\ \text{Ca}_{2.324}\text{Mg}_{0.334}\text{Cu}_{0.342}(\text{PO}_4)_2 \end{array}$	Decreasing of the unit cell parameters The occupation in the M5 site $({\rm Mg}^{2+} + {\rm Cu}^{2+})$. Compositions with $x({\rm Ca}^{2+}) < 2.571$ and $y({\rm Cu}^{2+} + {\rm Mg}^{2+}) > 0.286$ (2.2 mol.%) must contain impurity phase.	Co-existence of the ions in the structure facilitated the contact of Cu ²⁺ ions with the cell wall and thus enabling their damaging effect to the bacterial cell. The effect of the antimicrobial activity was tested on <i>S. aureus</i> and <i>E. coli</i> and it was rising with the increasing of the concentration of Mg ²⁺ /Cu ²⁺ The hemolysis rate of less than 5% was determined.	[20]
$Mg^{2+}/Mn^{2+}, Zn^{2+}$ and Fe^{3+}	$10 \; mol\% \; Mg^{2+} + 1 \\ mol\% \; of \; Mn^{2*}, \; up \; to \\ 3.75 \; mol\% \; of \; Zn^{2*} \\ and \; more \; than \; 2 \; mol \\ \% \; of \; Fe^{3*}$	Ca _{2.535} Mg _{0.3} Mn _{0.14} (FeZn) _{0.01} (PO ₄) ₂ Ca _{2.525} Mg _{0.3} (MnFeZn) _{0.05} (PO ₄) ₂ Ca _{2.515} Mg _{0.3} (MnFe) _{0.07} Zn _{0.01} (PO ₄) ₂ For studied compositions, the substitution limit for dopant ions is violated. The samples expected to contain impurities.	$\begin{array}{l} Ca_{2.87}Mg_{0.09}(MnFe)_{0.04}Zn_{0.05}P_2O_{2.78} \\ Ca_3Mg_{0.09}(MnFe)_{0.02}Zn_{0.03}P_2O_{2.6} \\ Ca_{3.04}Mg_{0.09}(MnFe)_{0.02}Zn_{0.05}P_2O_{2.6} \\ \textit{The stoichiometry is violated in the calculated formulas from the EDX data} \end{array}$	Formation of β -TCP and hydroxyapatite as the main crystalline phases. Compositions with $x(C\alpha^{2+}) < 2.571$ and $y(Mg^{2+}+Mn^{2+}+Zn^{2+}+Fe^{2+})>0.286$ must contain impurity phase.	Improving of the mechanical properties due to dense microstructure and good defined grain boundaries along with the absence of a cytotoxic effect was detected in the co-doped samples.	[21]
Zn ²⁺ / Fe ³⁺	From Zn ²⁺ :Fe ³⁺ (1:1) mol% To Zn ²⁺ :Fe ³⁺ (5:5) mol%	Ca _{2.94} Zn _{0.03} Fe _{0.03} (PO ₄) ₂ Ca _{2.70} Zn _{0.15} Fe _{0.15} (PO ₄) ₂ For the composition $(Zn^{2+};Fe^{3+})$ (5:5) mol% substitution limit is violated. The limiting composition is described by the formula $Ca_{2.643}(Zn + Fe)_{0.286}(PO_4)_2$	$\begin{array}{l} \text{Ca}_{2.94}\text{Zn}_{0.03}\text{Fe}_{0.03}(\text{PO}_4)_2 \\ \text{Ca}_{2.70}\text{Zn}_{0.16}\text{Fe}_{0.14}(\text{PO}_4)_2 \end{array}$	The occupation in the M5 site (Fe ³⁺ + Zn ²⁺) confirmed by the Rietveld refinement. Compositions with $x(Ca^{2+}) < 2.571$ and $y(Zn^{2+}+Fe^{2+})>0.286$ must contain impurity phase. The limit of β -TCP structure formation at $x(Zn^{2+}+Fe^{2+})<5$ mol% of dopant ions.	The cytotoxicity study revealed non-toxic nature of the co-doped samples by <i>in vivo</i> assay using zebrafish (Danio rerio).	[22]
Zn ²⁺ /Ag ⁺	Zn ²⁺ /Ag ⁺ (2.87:2.87) mol%	$Ca_{2.44}Zn_{0.373}Ag_{0.373}(PO_4)_2$ The substitution limit is violated. The limiting	Ca _{2.21} Zn _{0.26} Ag _{0.36} (PO ₄) ₂	The PXRD study recognized all the samples as single β -TCP phase. Smooth spherical morphology was	The study shows the 99.8% inhibition of <i>E. Coli</i> growth in the co-doped sample while in the single-doped Ca _{2.5} Ag _{0.38} (PO ₄) ₂ and Ca _{2.32} Ag _{0.75} (PO ₄) ₂	[23]

Table 1 (continued)

Doping ions	%, substitution	Calculated Expected formula The limit compositions were calculated by us using crystallochemical and literature data on the limits of substitution of calcium for other cations	Formula from the data (EDX or ICP-OS)	Crystal structure features. Our comments are in italics font. x, y – concentration of the host or dopant ions, respectively, in $Ca_xM_y(PO_4)_2$	Physical or biological enhancement by doping ions	Ref
		composition is described by the formula Ca _{2.571} Zn _{0.286} Ag _{0.286} (PO ₄) ₂		confirmed by TEM method. The co-doped sample with $x(Ca^{2+}) < 2.571$, $y(Zn^{2+}) > 0.286$ and $y(Ag) > 0.286$ contains the impurity phase.	phosphates the 82.5% and 99.9%, respectively, inhibition was revealed.	
Ag ⁺ /Zn ²⁺ Ag ⁺ / Cu ²⁺	Ag*:Zn ² + (9.09:15) mol.% Ag*:Cu ² + (9.09:15) mol.%	$Ca_{2.42}Ag_{0.27}Zn_{0.45}(PO_4)_2$ $Ca_{2.42}Ag_{0.27}Cu_{0.45}(PO_4)_2$ The substitution limit by Zn^{2+} and Cu^{2+} ions is violated. The limiting composition is described by the formula $Ca_{2.571}Zn_{0.286}Ag_{0.286}(PO_4)_2$ $Ca_{2.571}Cu_{0.286}Ag_{0.286}(PO_4)_2$	Not provided	The limit of β -TCP structure formation at 9.09 mol.% of dopant ions $(Ca_{2.60}Ag_{0.27}Zn_{0.27}(PO_4)_2 \text{ or } Ca_{2.60}Ag_{0.27}Zn_{0.27}(PO_4)_2 \text{ or } Ca_{2.60}Ag_{0.27}Cu_{0.27}(PO_4)_2)$ revealed by PXRD. At 12 mol.% the impurity $Ca_3Cu_3(PO_4)_4$ was detected. The co-doping ions Cu^{2+} and Zn^{2+} occupy the Ca5 site. Decreasing of the unit cell parameters up to 9.09 mol.% The leaching concentrations of Ag^+ ions were decreasing with the rising of co-doping ions content. The appearance of the impurity phase corresponding to excess the substitution limit x $(Zn^{2+}) \leq 0.286$, $x(Cu^{2+}) \leq 0.286$ and $y(Ag^+) < 0.286$.	The increase of the antimicrobial activity with the amount of divalent metal ions Cu^{2+} and Zn^{2+} were tested on $\textit{E. coli}$ and $\textit{S. aureus.}$ Ag $^+/\text{Zn}^{2+}$ and Ag $^+/\text{Cu}^{2+}$ co-substitutions display low cytotoxicity.	[24]
$\begin{array}{c} \text{Dy}^{3+} / \\ \text{Gd}^{3+} \end{array}$	From Dy ³⁺ :Gd ³⁺ (1.09:1.12) mol.% To Dy ³⁺ :Gd ³⁺ (4.38:4.42) mol.%	Not provided For some compositions, the substitution limit for $(Dy^{3+}+Gd^{3+})$ is violated. The limiting composition is described by the formula $Ca_{2.571}(Dy+Gd)_{0.286}(PO_4)_2$	$\begin{array}{l} \text{Ca}_{2.568} \text{Dy}_{0.142} \text{Gd}_{0.146} (\text{PO}_4)_2 \\ \text{Ca}_{1.284} \text{Dy}_{0.569} \text{Gd}_{0.575} (\text{PO}_4)_2 \end{array}$	The substitution limit of \sim 4.35 mol% was found. The excess of Dy ³⁺ /Gd ³⁺ ions leads to formation of DyPO ₄ and GdPO ₄ phases Compositions with $x(Ca) < 2.571$ and $y(Dy^{3+}+Gd^{3+})>0.286$ must contain impurity phase.	The photoluminescence properties were improved due to effective energy transfer process. The cell viability and in vitro imaging revealing that Gd^{3+} and Dy^{3+} co-substituted β -Ca ₃ (PO ₄) ₂ did not have a significant cytotoxic effect, making them a potential candidate for optical imaging and MRI and CT agents	[25]
Mn ²⁺ / Ni ²⁺	Mn ²⁺ :Ni ²⁺ (0.45:0.90) mol.% Mn ²⁺ :Ni ²⁺ (0.90:0.45) mol.%	$\begin{aligned} &\text{Ca}_{2.825}\text{Mn}_{0.059}\text{Ni}_{0.117}(\text{PO}_4)_2\\ &\text{Ca}_{2.825}\text{Mn}_{0.117}\text{Ni}_{0.059}(\text{PO}_4)_2.\\ &\textit{The limiting composition is not violated.} \\ &\textit{The limiting composition is described by the formula}\\ &\text{Ca}_{2.714}(\text{Mn}+\text{Ni})_{0.286}(\text{PO}_4)_2 \end{aligned}$	$\begin{array}{l} \text{Ca}_{2.825}\text{Mn}_{0.113}\text{Ni}_{0.037}(\text{PO}_4)_2 \\ \text{Ca}_{2.765}\text{Mn}_{0.057}\text{Ni}_{0.106}(\text{PO}_4)_2 \end{array}$	The impurity HAP phase was detected according to PXRD data. The co-doped samples with $x(Mn^{2^+}+Ni^{2^+}) \le 0.286$ expected to be single-phase. The presence of HAP is related to the synthesis conditions.	Co-doped samples did not possess effective antimicrobial activity against <i>E. coli, P. aeruginosa, S. aureus, E. faecalis, C. albicans, C. tropicalis.</i> The bone regeneration was superior in Ca _{2.825} Mn _{0.059} Ni _{0.117} (PO ₄) ₂ than in Ca _{2.825} Mn _{0.117} Ni _{0.059} (PO ₄) ₂ .	[26]
Ni ²⁺ / Fe ³⁺	From Ni ²⁺ :Fe ³⁺ (1.25: 1.25) mol.% to Ni ²⁺ :Fe ³⁺ (6.25: 6.25) mol. %	Ca _{2.95} Ni _{0.038} Fe _{0.038} (PO ₄) ₂ Ca _{2.53} Ni _{0.188} Fe _{0.188} (PO ₄) ₂ For all compositions, the substitution limit for $(Ni^{2+}+Fe^{3+})$ is violated. The limiting composition is described by the formula $Ca_{2.643}(Ni+Fe)_{0.286}(PO_4)_2$	$\begin{array}{l} \text{Ca}_{2,906} \text{Ni}_{0.037} \text{Fe}_{0.038} (\text{PO}_4)_2 \\ \text{Ca}_{2,535} \text{Ni}_{0.183} \text{Fe}_{0.188} (\text{PO}_4)_2 \end{array}$	The full occupation of the M5 site and partly occupation of the M4 site by $(\text{Fe}^{3+} + \text{Ni}^{2+})$ ions was confirmed by the Rietveld refinement. The decreasing of the unit cell parameters. The co-doped samples with $x(Ca^{2+}) < 2.571$ and $y(\text{Ni}^{2+} + \text{Fe}^{3+}) > 0.286$ must contain impurity phases. The impurity phases were detected in all samples.	Superior magnetic features and pronounced hyperthermia effect was detected. Fe ³⁺ /Ni ²⁺ co-substitutions display negligible toxicity.	[27]
Fe ³⁺ / Co ²⁺	From Fe ³⁺ :Co ²⁺ (1.25: 1.25) mol.% to Fe ³⁺ :Co ²⁺ (6.25: 6.25) mol. %	$\begin{array}{l} \text{Ca}_{2.905}\text{Co}_{0.038}\text{Fe}_{0.038}(\text{PO}_4)_2\\ \text{Ca}_{2.530}\text{Co}_{0.188}\text{Fe}_{0.188}(\text{PO}_4)_2\\ \text{For all compositions, the substitution limit for}\\ (\text{Co}^{2+}+\text{Fe}^{3+})\text{ is violated. The limiting composition}\\ \text{is described by the formula}\\ \text{Ca}_{2.643}(\text{Co}+\text{Fe})_{0.286}(\text{PO}_4)_2 \end{array}$	$\begin{array}{l} \text{Ca}_{2.906}\text{Co}_{0.037}\text{Fe}_{0.038}(\text{PO}_4)_2 \\ \text{Ca}_{2.529}\text{Co}_{0.188}\text{Fe}_{0.189}(\text{PO}_4)_2 \end{array}$	samples. The full occupation of the M5 site and partly occupation of the M4 site by $(Fe^{3+} + Co^{2+})$ ions was confirmed by the Rietveld refinement. The decreasing of the unit cell parameters. The co-doped samples with $x(Ca^{2+}) < 2.571$ and $y(Co^{2+} + Fe^{3+}) > 0.286$ must contain	The study shows the inhibition of <i>E. Coli S. aureus</i> growth. A hemolytic rate <5% was observed for all investigated compositions.	[28]

	Ref	[29]
	Physical or biological enhancement by doping ions	All samples display negligible toxicity on the MG-63 cells.
	Crystal structure features. Our comments are in italics font. x, y – concentration of the host or dopant ions, respectively, in $C\alpha_s M_s(PO_d)_2$	impurity phase. The inpurity phases were detected in all samples. The full occupation of the M5 site and partly occupation of the M4 site by $(Fe^{3+} + Mn^{2+})$ ions was confirmed by the Rietveld refinement. The decreasing of the unit cell parameters. The co-doped samples with $x(Ca^{2+}) < 2.571$ and $y(Mn^{2+} + Fe^{3+}) > 0.286$ must contain impurity phase. The impurity phases were detected in all samples.
	Formula from the data (EDX or ICP-OS) Our comments are in italics x, y – concentration of the h respectively, in Ca ₂ M ₃ (PO ₄)	Ca _{2,59,9} Mn _{0,037} Fe _{0,036} (PO ₄₎₂ Ca _{2,534} Mn _{0,184} Fe _{0,188} (PO ₄₎₂
	Calculated Expected formula The limit compositions were calculated by us using crystallochemical and literature data on the limits of substitution of calcium for other cations	Ga_205Mn _{0.038} Fe _{0.038} (PO ₄) ₂ Ga_2530Mn _{0.138} Fe _{0.038} (PO ₄) ₂ For all compositions, the substitution limit for (Mn^2++Fe^3+) is violated. The limiting composition is described by the formula Ca_2 $\epsilon_{43}(Mn+Fe)_0$. $286(PO_4)_2$
tmued)	%, substitution	From Fe ³⁺ :Mn ²⁺ (1.25: 1.25) mol.% to Fe ³⁺ :Mn ²⁺ (6.25: 6.25) mol. %
Table 1 (continued)	Doping ions	$Fe^{3+/}\\ Mn^{2}+$

PXRD phase analysis, compositions (1) and (4) were single-phase. Their PXRD patterns contain reflections belonging only to the $\beta\text{-}Ca_3(PO_4)_2$ -type structure [31]. PXRD patterns of compositions (2), (3) and (5) also contain Zn₃(PO₄)₂, Ca₃Cu₃(PO₄)₄ or Ca₂P₂O₇ impurity phases (Table 1) in addition to $\beta\text{-}Ca_3(PO_4)_2$ reflections. To estimate the quantity of phases in (2), (3) and (4) samples, it was assumed:

- 1) in $Ca_{3-x}Zn_x(PO_4)_2$ [32], $Ca_{3-x}Cu_x(PO_4)_2$ [33] and $Ca_{3-x}Sr_x(PO_4)_2$ [34] the solid solutions are formed with the maximum possible concentration of Zn^{2+} , Cu^{2+} and Sr^{2+} , respectively, or $Zn^{2+}+Cu^{2+}$, $Cu^{2+}+Sr^{2+}$ and $Mn^{2+}+Sr^{2+}$, respectively;
- 2) these solid solutions have the β -Ca₃(PO₄)₂-type structure. The formulas for limit compositions in Table 2 are marked in bold. It should be noted that samples (3) and (4) contained very small amounts of impurity phases (\leq 3.2% (w)). Such quantities of impurities should not significantly effect on the antimicrobial activity.

The obtained results of the quantitative phase analysis are in a good agreement with the FT-IR data (see below). The unit cell parameters and volume (Table 2) of the as-synthesized samples directly depend on the radii of the introduced ions. These parameters for β -TCP and β -TCP-Cu are comparable with the results reported previously on pure β -TCP [35] and Cu-doped β-TCP phosphate Ca₉Cu_{1.5}(PO₄)₇ [33], respectively. The substitution $Ca^{2+} \rightarrow Cu^{2+}$ led to noticeable decreasing of the unit cell parameters, according to smaller ionic radius of Cu^{2+} ($r_{VI} = 0.73 \text{ Å}$) compared to Ca^{2+} ($r_{VI} = 0.73 \text{ Å}$) [36] (Table 2). Further, β -TCP-Cu sample can serve as a reference for evaluating the changes of the unit cell parameters for co-doped samples. The impurity Ca₃Cu₃(PO₄)₄ phase was taken into account during the Le Bail decomposition. Therefore, it does not contribute or distort on the refined parameters for β -TCP-Cu. In $\beta\text{-TCP-Cu}+Zn$ the unit cell parameters are similar to $\beta\text{-TCP-Cu}$ since the ionic radius of Zn^{2+} ($r_{VI} = 0.74$ Å) is very close to Cu^{2+} . According to Ref. [20], the ions with small ionic radii can be only located jointly in the octahedral M5 site of the $\beta\text{-TCP}$ structure (see Fig. 6 below). The limit of the β -TCP structure formation in Ca_{3-x}M_x(PO₄)₂ was found to be $x \le$ 0.429 (or $x \le 1$ in $Ca_{10.5-x}M_x(PO_4)_2$, when Z = 6) (Table 1). In β-TCP-Cu+Zn the substitution limit for (Cu²⁺+Zn²⁺) was violated. So, the excess of Zn²⁺ ions formed the impurity Zn₃(PO₄)₂ phase (Table 2).

The noticeable increasing of the unit cell parameters was found in $\beta\text{-TCP-Cu+Sr}$ sample (Table 2). According to Ref. [19], the preferential occupation of Sr^{2+} ions is in the M4 site, while Cu^{2+} ions are located in the M5 site. The incorporation of Sr^{2+} ions results in the enlargement of the coordination polyhedra, and leads to growth of the unit cell. This enlargement along with the absence of competition in occupation of the M5 site, avoids carrying out co-substitutions to a greater extent. This fact is confirmed by the absence of impurities in $\beta\text{-TCP-Cu+Sr}$ sample. The co-doping was performed up to 8.3 mol.% of each Cu^{2+} and Sr^{2+} ions (Table 2).

The difference in the ionic radii value of Mn^{2+} ($r_{VI}=0.84$ Å) [36] and Cu^{2+} results in the enlargement of the unit cell parameters in β -TCP-Mn+Sr in comparison with β -TCP-Cu+Sr (Table 2). In this case, the co-doping of Mn^{2+} along with Sr^{2+} ions allows to obtain β -TCP structure without of impurities of different phosphate phases.

3.2. SEM observations

SEM images of the as-synthesized samples are shown in Fig. 2. The shape and the morphology of the particles are close to each other. The decreasing trend of the particles size in the co-doped samples can be seen in comparison with single doped $\beta\text{-TCP-Cu}$ (Fig. 2). An EDX analysis of the samples was used to confirm the chemical composition and the presence of $\text{Cu}^{2+}/\text{Sr}^{2+}/\text{Mn}^{2+}/\text{Zn}^{2+}$ ions in the solid solutions. The measurements were performed for 8 points of each crystallite sample. Using EDX, the Ca : Cu: Sr : Mn : Zn : P ratios have been obtained which were close to the expected bulk composition. The results of EDX analysis are shown in Table 3 as the obtained chemical compositions along with

Table 2Initial mixtures, refined phase composition and results of the quantitative phase analysis for prepared samples.

Nº	Abbreviation	Composition of initial mixture	Refined Phase composition	wt% (JANA 2006)	a, Å	c, Å	<i>V</i> , Å ³
1	β-ТСР	β-Ca ₃ (PO ₄) ₂	β-Ca ₃ (PO ₄) ₂	100	10.439(1)	37.395(5)	3526.1(2)
2	β-TCP-Cu	$Ca_{2.5}Cu_{0.5}(PO_4)_2$	Ca _{2.571} Cu _{0.429} (PO ₄) ₂	97	10.334(9)	37.141(7)	3434.4(3)
			$Ca_3Cu_3(PO_4)_4$	3			
3	β -TCP-Cu+Zn	$Ca_{2.5}Cu_{0.25}Zn_{0.25}(PO_4)_2$	$Ca_{2.571}Cu_{0.257}Zn_{0.172}(PO_4)_2$	96.4	10.337(6)	37.189(8)	3442.1(5)
			$Zn_3(PO_4)_2$	2.6			
			$Ca_2P_2O_7$	1			
4	β -TCP-Cu+Sr	$Ca_{2.5}Cu_{0.25}Sr_{0.25}(PO_4)_2$	$Ca_{2.5}Cu_{0.25}Sr_{0.25}(PO_4)_2$	100	10.347(9)	37.271(7)	3449.5(2)
5	β-TCP- Mn+Sr	$Ca_{2.5}Mn_{0.25}Sr_{0.25}(PO_4)_2$	$Ca_{2.5}Mn_{0.25}Sr_{0.25}(PO_4)_2$	99	10.355(2)	37.284(3)	3455.7(8)
			$Ca_2P_2O_7$	1			

^{*-} phase with the β-Ca₃(PO₄)₂-type structure are marked in bold.

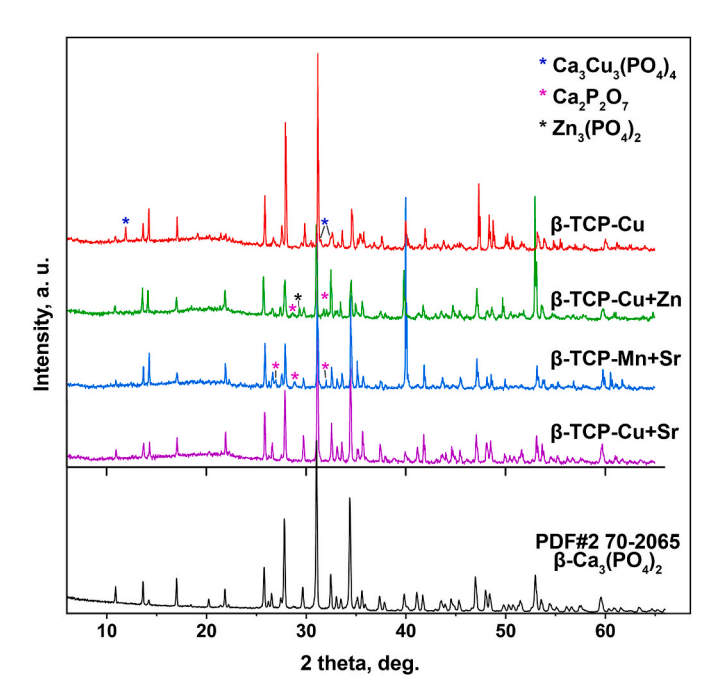


Fig. 1. PXRD patterns of β-TCP-Cu, β-TCP-Cu+Zn, β-TCP-Cu+Sr and β-TCP-Mn+Sr samples along with PDF#2 70–2065 card (β-Ca₃(PO₄)₂). The asterisks mark the impurity $Ca_2P_2O_7$, $Ca_3Cu_3(PO_4)_4$ and $Zn_3(PO_4)_2$ phases.

the expected. Fig. 3 shows the enlarged SEM images (at 10 μ m resolution) of the particles. The excess of the ionic species Cu²⁺ and Zn²⁺ concentration deposits at the surface of the larger particles along with the isthmuses between them.

3.3. FT-IR spectroscopy

The FT-IR spectra of the synthesized samples are shown in Fig. 4. Infrared spectroscopy is a useful tool for the rapid evaluation of the resulting phase mixtures. It allows to reveal pyrophosphate phases, admixture and the presence of HAP or Ca(OH)₂ OH-group. However, if the mixture consists of different orthophosphates, for example β -TCP, apatite, Cu₃(PO₄)₂ or Zn₃(PO₄)₂, the overlapping both in stretching and in bending vibrations of PO³₄ units takes place, and the phase identification on IR spectroscopy data is difficult or even impossible.

Four spectra of the samples synthesized using high temperature solid-state reactions are very similar due to the predominance of $\beta\text{-TCP}$ phase (Fig. 4). However, one of them ($\beta\text{-TCP-Cu+Sr}$) corresponds to pure $\beta\text{-TCP}$ phase [5] and the other three spectra contain weak bands of Ca₂P₂O₇. The bands of ν_s P - O - P bridges are located at different wavenumbers for $\beta\text{-TCP-Mn+Sr}$ (752 cm $^{-1}$) and for $\beta\text{-TCP-Cu+Zn}$ (729 cm $^{-1}$). This may indicate different modifications of the calcium pyrophosphate Ca₂P₂O₇ as an admixture: $\alpha\text{-Ca}_2$ P₂O₇ in $\beta\text{-TCP-Mn+Sr}$ and $\beta\text{-Ca}_2$ P₂O₇ in $\beta\text{-TCP-Cu+Zn}$ [37].

Compared with the spectrum of the co-doped samples, the IR spectrum of $\beta\text{-TCP-Cu}$ does not contain the bands of pyrophosphates. The bands of small admixture of Ca₃Cu₃(PO₄)₂ the fully overlapped by $\beta\text{-TCP}$ bands and could not be revealed in IR spectrum. It should be noted that IR spectrum and quantitative X-ray analysis confirm the presence of Ca₂P₂O₇ in $\beta\text{-TCP-Cu+Zn}$ and $\beta\text{-TCP-Mn+Sr}$ samples.

The region 4000–1300 $\rm cm^{-1}$ are free of absorption bands, which means the absence of any $\rm H_2O$ molecules or $\rm OH^-$ groups in crystal structures of mixed phases.

3.4. Antibacterial activity study

The obtained experimental data show that the incorporation of Cu^{2+} , Zn^{2+} , Mn^{2+} and Sr^{2+} ions into the $\beta\text{-Ca}_3(\text{PO}_4)_2$ structure always inhibits the growth of various organisms. The growth (%) and growth inhibition (%) of each microorganism with respect to the different compositions of compounds are detailed in Table 4 and Fig. 5.

4. Discussion

For understanding the obtained biological properties, it is advisable to consider the crystal chemical features of calcium substitution for divalent ions during the formation of solid solutions with $\beta\text{-TCP-type}$ structure. In the $\beta\text{-Ca}_3(PO_4)_2$ structure (space group (SG), R3c,~Z=21), Ca $^{2+}$ ions occupy five crystallographic sites M1, M2, M3, M4 and M5 [31]. Eight-fold M1, M2, M3 and six-fold M5 positions are completely occupied by Ca $^{2+}$ cations. The six-fold M4 site is half occupied by Ca $^{2+}$ cations. Taking these structural features into account, the crystal chemical formula of the $\beta\text{-Ca}_3(PO_4)_2$ structure can be written as follows: Ca(1)_3Ca(2)_3Ca(3)_3Ca(4)_0.5[1](4)_0.5Ca(5)[1](6)(PO_4)_7 (Z=6). The structure is built up by two columns-PO_4-Ca(4)-Ca(5)-[1](6)-PO_4- ... (type A column) and-PO_4-Ca(1)-Ca(3)-Ca(2)-PO_4- (type B column). Columns A and B form two layers (Fig. 6).

One of the layers is built only from columns of type B (Fig. 6a) and in the second layer – columns A and B alternate (Fig. 6b). Calcium cations in the M1, M2 and M3 sites have eight oxygen atoms each in the nearest environment (Fig. 7) with an average distance $d_{<\text{Ca-O>}}=2.505~\text{Å},~2.486~\text{Å}$ and 2.536 Å, respectively. Fig. 7 include the average distances in the M1-M3 polyhedra for $\beta\text{-Ca}_3(PO_4)_2$ [35] Ca9.5Cu(PO_4)7 [38], Ca9.615Mn_0.885(PO_4)7 [39] and Ca9Cu_1.5(PO_4)7 [33] structures. In the M4 position, the Ca^2+ ion has three oxygen atoms in the nearest environment at a distance of 2.538 Å. Other oxygen atoms are removed (d_{Ca}_{(4)-O}=3.041~\text{Å} and 3.222 Å) (Fig. 8).

In the M5 position, the Ca^{2+} ion has an octahedral environment with $d_{<Ca(5)-O>}=2.263$ Å (Fig. 8). In this octahedra, the Ca–O distance is less than the sum of the ionic radii [36] of calcium and oxygen (1.00 Å $(r_{VI}Ca^{2+})+1.40$ Å $(r_{VI}O^{2-})=2.4$ Å), which creates the stress in the structure. When Ca^{2+} ($r_{VI}=1.00$ Å) is replaced by an ion with a smaller radius, for example, Cu^{2+} ($r_{VI}=0.73$ Å), the stress in the structure can be removed, and the structure becomes more stable. The M5–O distances in structures with Cu^{2+} and $Ca_{9.615}Mn_{0.885}(PO_4)$ 7 [38] and $Ca_{9.615}Mn_{0.885}(PO_4)$ 7 [39] structures also

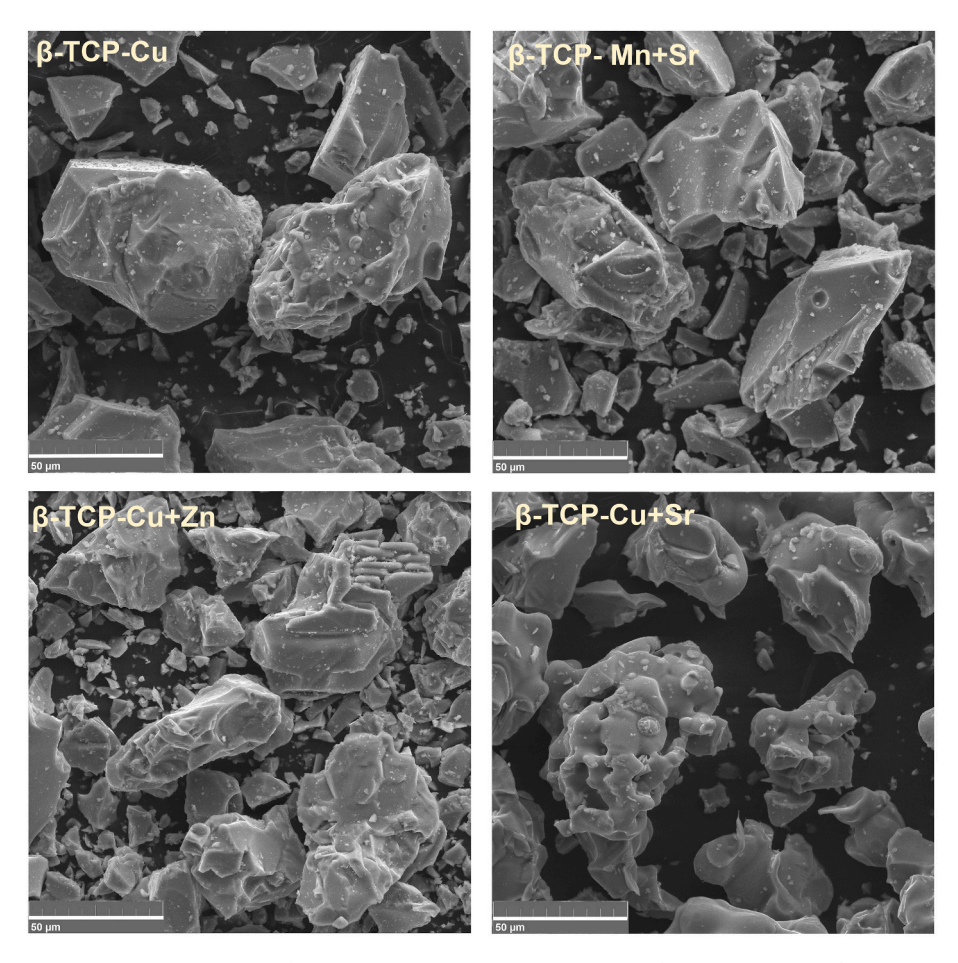


Fig. 2. SEM images of β -TCP-Cu, β -TCP-Cu+Zn, β -TCP-Cu+Sr and β -TCP-Mn+Sr samples.

Table 3Chemical composition of the synthesized samples obtained by EDX data. The values are given with a relative error of 0.05%.

Abbreviation	Formula of initial mixture	Nominal Dopant(s)/(Ca + dopant(s)) (percentage)	Calculated formula from EDX data	EDX Dopant(s)/(Ca + dopant(s)) (percentage)	EDX (Ca ²⁺ +dopant (s))/P, (molar ratio)
β-ТСР	β-Ca ₃ (PO ₄) ₂	0	Ca _{2,99} (PO ₄) ₂		1.495
β-TCP-Cu	$Ca_{2.5}Cu_{0.5}(PO_4)_2$	16.7 mol.%	$Ca_{2.61}Cu_{0.39}(PO_4)_2$	13 mol.%	1.5
β -TCP- Cu+Zn	$Ca_{2.5}Cu_{0.25}Zn_{0.25}(PO_4)_2$	8.3 mol.% Cu^{2+} and 8.3 mol. % Zn^{2+}	$Ca_{2.23}Cu_{0.31}Zn_{0.35}(PO_4)_2$	$10.3 \text{ mol.}\% \text{ Cu}^{2+} \text{ and } 11.7$ mol.% Zn^{2+}	1.445
$\beta\text{-TCP-Cu+Sr}$	$Ca_{2.5}Cu_{0.25}Sr_{0.25}(PO_4)_2$	$8.3 \text{ mol.}\% \text{ Cu}^{2+} \text{ and } 8.3 \text{ mol.}$ % Sr^{2+}	$Ca_{2.40}Cu_{0.27}Sr_{0.24}(PO_4)_2$	9 mol.% Cu^{2+} and 8 mol.% Sr^{2+}	1.475
$_{\substack{\beta\text{-TCP-}\\Mn+Sr}}$	$Ca_{2.5}Mn_{0.25}Sr_{0.25}(PO_4)_2$	8.3 mol.% Mn^{2+} and 8.3 mol. % Sr^{2+}	$Ca_{2.5}Mn_{0.26}Sr_{0.24}(PO_4)_2$	$8.7~\text{mol.}\%~\text{Mn}^{2+}$ and $8~\text{mol.}\%~\text{Sr}^{2+}$	1.5

decrease in contrast to $Ca_9Cu_{1.5}(PO_4)_7$ [33] (Fig. 8).

The $\text{Ca}^{2+} \to \text{Cu}^{2+}$ substitution in the $\beta\text{-Ca}_3(\text{PO}_4)_2$ structure [31] results in the formation of $\text{Ca}_{10.5-x}\text{Cu}_x(\text{PO}_4)_7$ solid solutions [33,40,41]. Nord [41] has found that solid solutions exist in the range of compositions with $0 \le x \le 1.25$. Belik et al. [33] showed that solid solutions are formed in $0 \le x \le 1.5$ range. Romdhane et al. [42] investigated solid solutions $\text{Ca}_{10.5-x}\text{Cu}_x(\text{PO}_4)_7$ only in $0 \le x \le 1$ composition range. The distribution of Cu^{2+} ions over the crystallographic sites in the $\beta\text{-Ca}_3(\text{PO}_4)_2$ structure (Z = 21, SG R3c) [31] ($\beta\text{-Ca}_{10.5}(\text{PO}_4)_7$, Z = 6) was studied by UV-VIS and EPR [40,42] methods, single Rietveld [33,38,43] refinement, and Rietveld and EPR [44] methods. Romdhane et al. [42] suggested that Cu^{2+} ions are located in the M3 sites. The catalytic activity study of $\text{Ca}_{10.5-x}\text{Cu}_x(\text{PO}_4)_7$ ($0 \le x \le 1$) [40] suggested that Cu^{2+} ions occupy two sites: M4 and M5 in the $\beta\text{-Ca}_3(\text{PO}_4)_2$ structure. In this case, the Cu^{2+} ions in the M4 positions play the main role in catalytic

processes. According to structural studies of $Ca_{9.5}Cu(PO_4)_7$ (sintered at 973 – 1173 K with subsequent slow cooling), Cu^{2+} ions are completely located in the M5 sites [17,24]. When $Ca_{9.5}Cu(PO_4)_7$ was quenched from 1173 K into the air, a different distribution of Cu^{2+} was observed [33]. In this case, M5 sites are occupied by $0.79Cu^{2+} + 0.21Ca^{2+}$. The remaining amount of Cu^{2+} ions are located in the M4 sites. Yanov [44] et al. also have noted the presence of impurity amounts of Cu^{2+} in the M4 positions in $Ca_{10}Cu^+(PO_4)_7$. It follows from the above data that the location of Cu^{2+} ions in the β - $Ca_3(PO_4)_2$ structure depends significantly both on the preparation method and on the Cu^{2+} concentration in the sample.

Taking into account the crystal-chemical features of the $\beta\text{-Ca}_3(PO_4)_2$ -type structure, it can be expected that Cu^{2+} will replace Ca^{2+} in the M5 sites upon $Ca^{2+} \to Cu^{2+}$ substitution in $Ca_{10.5-x}Cu_x(PO_4)_7$ (0 $\leq x \leq$ 1). Such substitution corresponds to the crystal chemical formula Ca(1)₃Ca (2)₃Ca(3)₃Ca(4)_{0.5}[4)_{0.5}Ca(5)_{1-x}Cu(5)_x(PO_4)₇. The limit composition

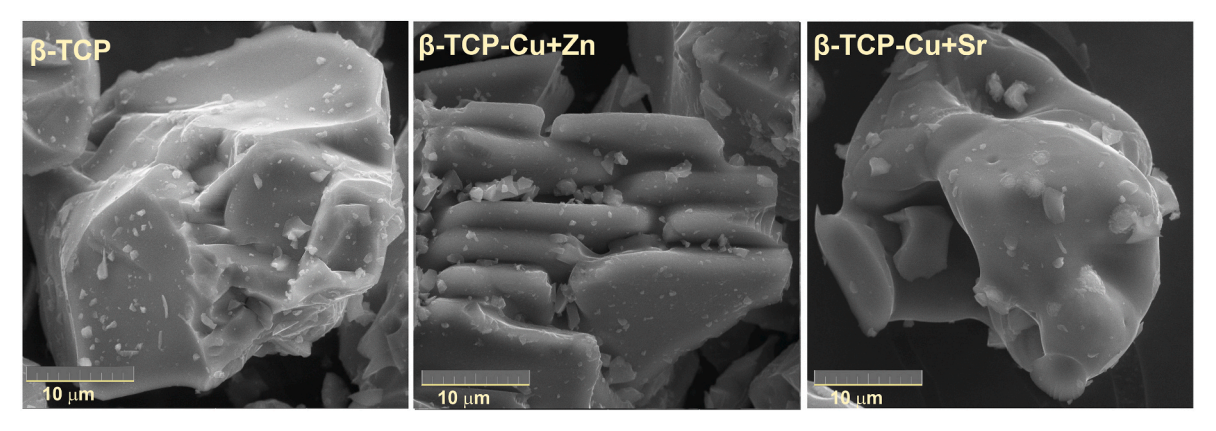


Fig. 3. SEM images β-TCP, β-TCP-Cu+Zn and β-TCP-Cu+Sr samples at 10 μ m resolution.

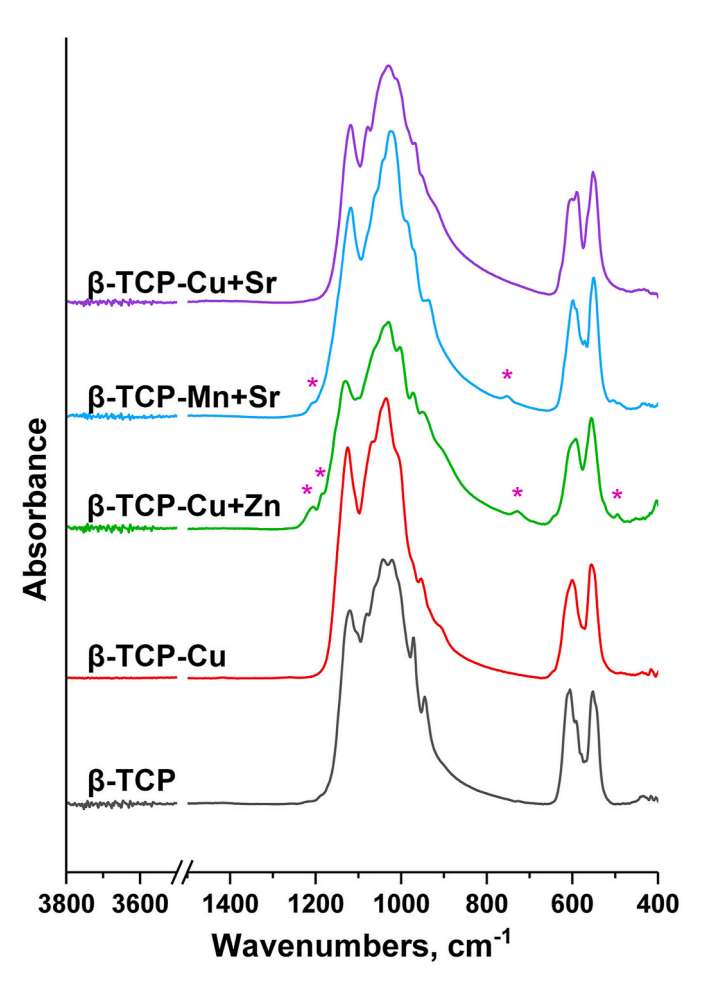


Fig. 4. FT-IR spectra of β-TCP, β-TCP-Cu, β-TCP-Cu+Zn, β-TCP-Cu+Sr and β-TCP-Mn+Sr samples, magenta asterisks – the bands belong to α - and/or β- $Ca_2P_2O_7$.

in $Ca_{10.5-x}Cu_x(PO_4)_7$ (x=1) is described as $Ca_{9.5}Cu(PO_4)_7$ ($Ca_{2.714}Cu_{0.286}(PO_4)_2$). It was found that the Cu^{2+} ions are located in the M5 sites [38,43] in this composition. It can be assumed that Cu^{2+} occupy the M5 sites in $Ca_{10.5-x}Cu_x(PO_4)_7$ ($0 \le x \le 1$) as in $Ca_{9.5}Cu(PO_4)_7$ ($Ca_{2.714}Cu_{0.286}(PO_4)_2$) [38,43] since the X-ray diffraction characteristics (a, c, and V) vary linearly [33] in $Ca_{10.5-x}Cu_x(PO_4)_7$ at $0 \le x \le 1$ (slow cooling to room temperature). However in $Ca_{10.5-x}Cu_x(PO_4)_7$ ($0 \le x \le 1$, quenching into air) Cu^{2+} occupy the M4 and M5 sites.

In $Ca_{10.5-x}Cu_x(PO_4)_7$ in the range $1 \le x \le 1.5$, the crystallographic characteristics also change linearly, however, with different trends

Table 4

Antibacterial test performed on β -TCP, β -TCP-Cu, β -TCP-Cu+Zn, β -TCP-Cu+Sr and β -TCP-Mn+Sr. In this experiment, the different microorganisms were considered positive controls of the experiment. The table shows the OD 600 nm, the standard deviation, the % growth, and the % growth inhibition. The reported values are expressed as mean values \pm standard deviation of 3 independent experiments.

Samples	OD 600 nm	SD	% growth	% inhibition
S. aureus				
CTR+	0.87	0.02	100.0	0.0
β-ТСР	0.62	0.05	71.8	28.2
β-TCP-Cu	0.46	0.04	52.9	47.1
β -TCP-Cu+Zn	0.35	0.03	40.1	59.9
β -TCP-Cu+Sr	0.07	0.02	8.1	92.0
β-TCP-Mn+Sr	0.37	0.01	42.2	57.8
P. aeruginosa			-	
CTR+	0.85	0.03	100.0	0.0
β-TCP	0.52	0.09	60.7	39.3
β-TCP-Cu	0.41	0.02	47.8	52.2
β -TCP-Cu+Zn	0.18	0.01	20.7	79.3
β -TCP-Cu+Sr	0.04	0.02	4.5	95.5
β-TCP-Mn+Sr	0.06	0.02	7.1	92.9
E. coli			-	
CTR+	1.03	0.17	100.0	0.0
β-ТСР	1.01	0.11	97.9	2.1
β-TCP-Cu	0.74	0.11	72.3	27.7
β -TCP-Cu+Zn	0.67	0.08	64.8	35.2
β -TCP-Cu+Sr	0.36	0.01	35.2	64.9
β -TCP-Mn+Sr	0.83	0.31	81.0	19.0
E. faecalis				
CTR+	0.53	0.07	100.0	0.0
β-TCP	0.43	0.07	81.5	18.5
β-TCP-Cu	0.33	0.01	62.8	37.2
β -TCP-Cu+Zn	0.12	0.04	22.6	77.4
β -TCP-Cu+Sr	0.02	0.01	3.7	96.3
β-TCP-Mn+Sr	0.17	0.01	32.6	67.4
C. albicans				
CTR+	0.46	0.05	100.0	0.0
β-ТСР	0.39	0.06	85.8	14.2
TCP-Cu	0.20	0.01	43.6	56.5
β -TCP-Cu+Zn	0.23	0.05	49.1	50.9
β -TCP-Cu+Sr	0.13	0.05	29.1	70.9
β -TCP-Mn+Sr	0.27	0.06	58.1	41.9

compared to $0 \le x \le 1$ compositions [33]. It is expected that Cu^{2+} ions occupy M4 and M5 sites at $1 \le x \le 1.5$ $Ca_{10.5-x}Cu_x(PO_4)_7$ since it was approved in the limit composition $Ca_9Cu_{1.5}(PO_4)_7$ ($Ca_{2.571}Cu_{0.429}(PO_4)_2$) [33]. The corresponding crystal chemical formula is $Ca(1)_3Ca(2)_3Ca(3)_3Ca(4)_{0.5-x}Cu(4)_x \square (4)_{0.5}Ca(5)_{1-x}Cu (5)_x(PO_4)_7$. Previously, using the Rietveld refinement it was shown that

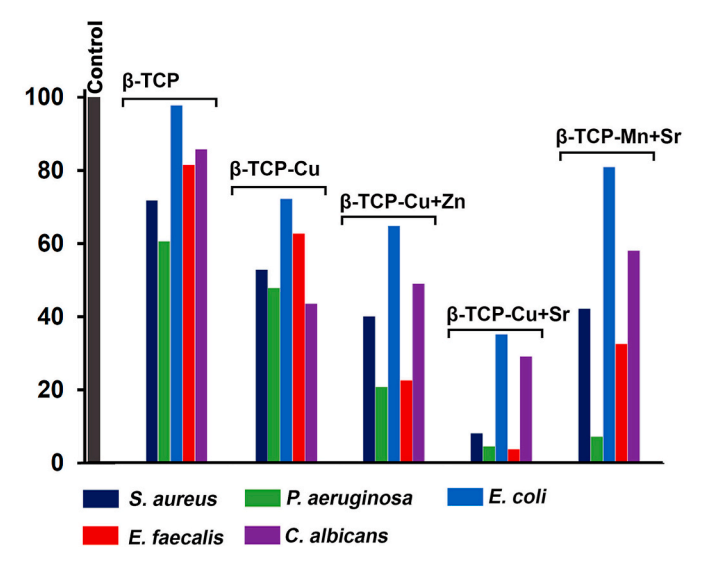


Fig. 5. Study of the growth of S. aureus, P. aeruginosa, E. coli, E. faecalis, C. albicans at 37 °C for 24 h in the presence of $\beta\text{-TCP}$, $\beta\text{-TCP-Cu}$, $\beta\text{-TCP-Cu+Zn}$, $\beta\text{-TCP-Cu+Sr}$ and $\beta\text{-TCP-Mn+Sr}$. The bacterium grown on its own represents the positive control of the experiment. The graph shows the mean values OD 600 nm \pm standard deviation of 3 independent experiments.

 $M=Mn^{2+}$, Zn^{2+} ions in $Ca_{9.5}M(PO_4)_7$ [45] completely occupy the Ca(5) octahedral sites, as in the analogous Cu^{2+} -doped compounds. The phase diagrams studied in $Ca_3(PO_4)_2$ – $Zn_3(PO_4)_2$ [46], ZnO–CaO– P_2O_5 [47] systems and in $Ca_{3-x}Zn_x(PO_4)_2$ [32] solid solutions revealed that $Ca_{9.5}Zn$ (PO_4) $_7$ is the limit composition during the $Ca^{2+} \rightarrow Zn^{2+}$ replacement in β- $Ca_3(PO_4)_2$.

In the β -Ca₃(PO₄)₂-type structure the manganese ions Mn²⁺ occupy the M5 sites in Ca_{9.615}Mn_{0.885}(PO₄)₇ [39] and Ca_{9.5}Mn(PO₄)₇ (Ca_{2.714}Mn_{0.286}(PO₄)₂) [48]. The existence limit of Ca_{3-x}Mn_x(PO₄)₂

solid solutions has not been established yet. Since $Ca_{9.5}Mn(PO_4)_7$ ($Ca_{2.714}Mn_{0.286}(PO_4)_2$) composition has been reliably characterized [48], it can be stated that $Ca_{3-x}Mn_x(PO_4)_2$ solid solutions exist at $0 \le x \le 0.286$ range.

The $Ca^{2+} \rightarrow Sr^{2+}$ substitution in $Ca_{3-x}Sr_x(PO_4)_2$ solid solutions occurs in a wide range $0 \le x \le 2.286$ with the formation of noncentrosymmetric phases (0 $\leq x \leq$ 1.286, SG R3c), centrosymmetric phases $(1.857 \le x \le 2.286, SG R\overline{3} m)$ and two-phase region $(1.429 \le x \le 3.286, SG R\overline{3} m)$ 1.714. SG $R3c + R\overline{3}m$) [34]. Non-centrosymmetric and centrosymmetric phases are very difficult to distinguish by X-ray diffraction due to the similarity of the PXRD patterns. For this reason, it can be assumed that solid solutions are formed for compositions with 0 < x < 2.286. However, in the presence of anomalies in the properties of Ca_{3-x}Sr_x(PO₄)₂ solid solutions, their symmetry and the regions of existence of non-centrosymmetric and centrosymmetric phases must be taken into account. The distribution of Sr2+ ions over crystallographic sites was studied only for the following compositions Sr_{1.75}Ca_{1.25}(PO₄)₂:Eu²⁺ [49] and $Ca_{2.87}Sr_{0.13}(PO_4)_2$ [50]. It should be noted that in $Sr_{1.75}Ca_{1.25}(PO_4)_2$: Eu^{2+} [49], Sr^{2+} ions occupy the M1, M2, M3 and M4 sites jointly with Ca^{2+} ions. Nevertheless, the distribution of Sr^{2+} in Ca_{2.87}Sr_{0.13}(PO₄)₂ [50] was determined incorrectly. The authors claimed the occupation of small octahedral M5 sites [50] by large Sr²⁺ ions with $r_{VI} = 1.18 \text{ Å } [36]$ ionic radii.

There are no reliable data on the distribution of Sr^{2+} ions over crystal sites in $Ca_{3_x}Sr_x(PO_4)_2$ with the β - $Ca_3(PO_4)_2$. However, such data are known for isostructural $Ca_{3_x}Pb_x(VO_4)_2$ [51] solid solutions. Since the ionic radii of Sr^{2+} ($r_{VIII}=1.26$ Å) and Pb^{2+} ($r_{VIII}=1.29$ Å) differ insignificantly, it can be assumed that in $Ca_{3_x}Sr_x(PO_4)_2$ and $Ca_{3_x}Pb_x(VO_4)_2$ solid solutions, the distribution of Sr^{2+} and Pb^{2+} through the crystal sites will be similar. Taking this assumption into account, we can state that Sr^{2+} ions jointly with Ca^{2+} will occupy only M4 site in $Ca_{3_x}Sr_x(PO_4)_2$ at $0 \le x \le 0.143$. In the limit composition $Ca_{2.857}Sr_{0.143}(PO_4)_2$ the M4 sites are completely occupied by Sr^{2+} . For compositions with x > 0.143, the Sr^{2+} ions will predominantly occupy

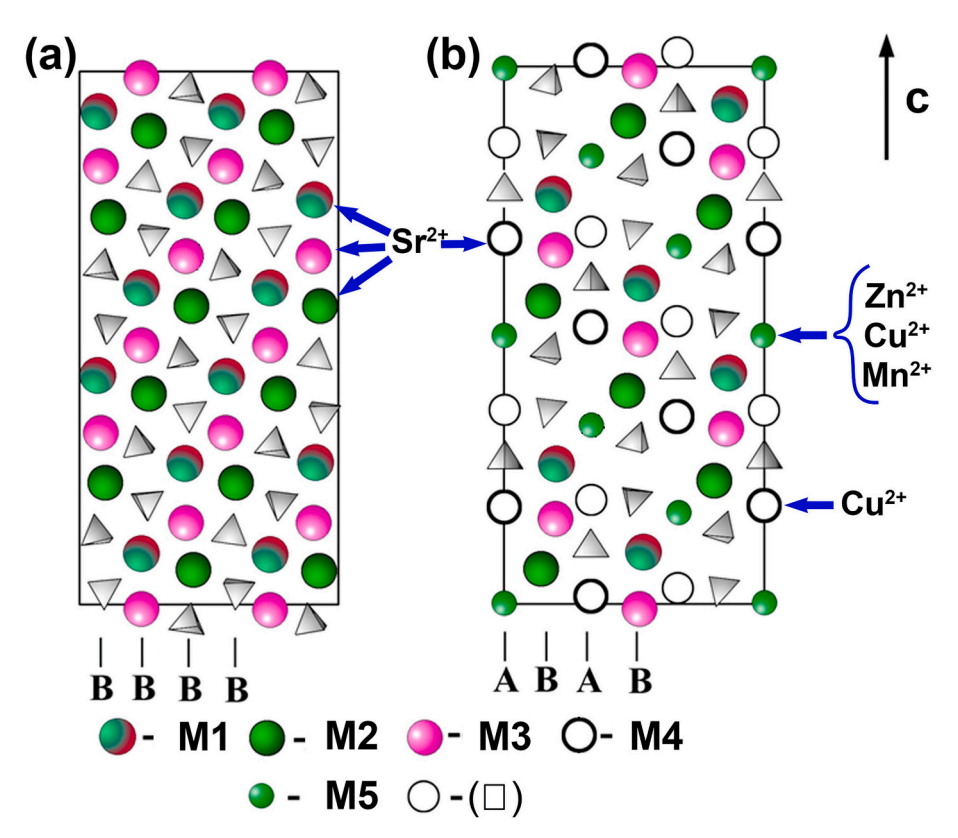


Fig. 6. Projections of β -Ca₃(PO₄)₂ structure along [210]: layers with only B columns (a); layers with A and B columns (b).

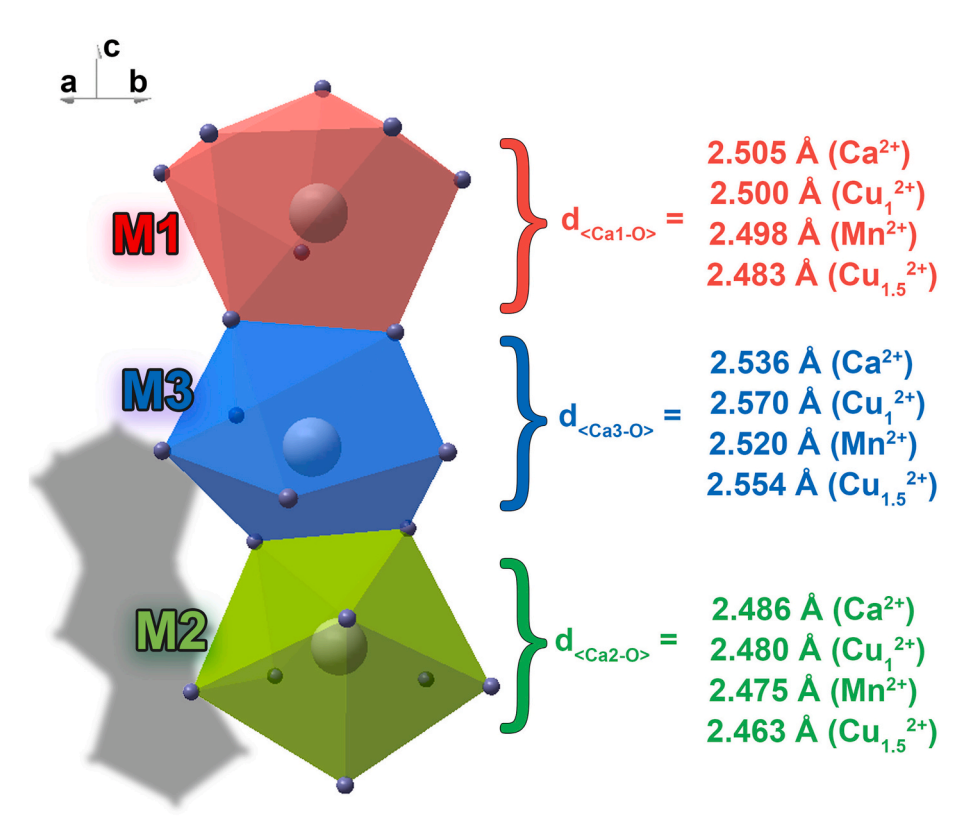


Fig. 7. Alternation of CaO_8 polyhedra in the β - $Ca_3(PO_4)_2$ -type structure along with the average distances in the M1-M3 polyhedra for β - $Ca_3(PO_4)_2$ [35] $Ca_{9.5}Cu(PO_4)_7$ [38], $Ca_{9.615}Mn_{0.885}(PO_4)_7$ [39] and $Ca_9Cu_{1.5}(PO_4)_7$ [33] structures.

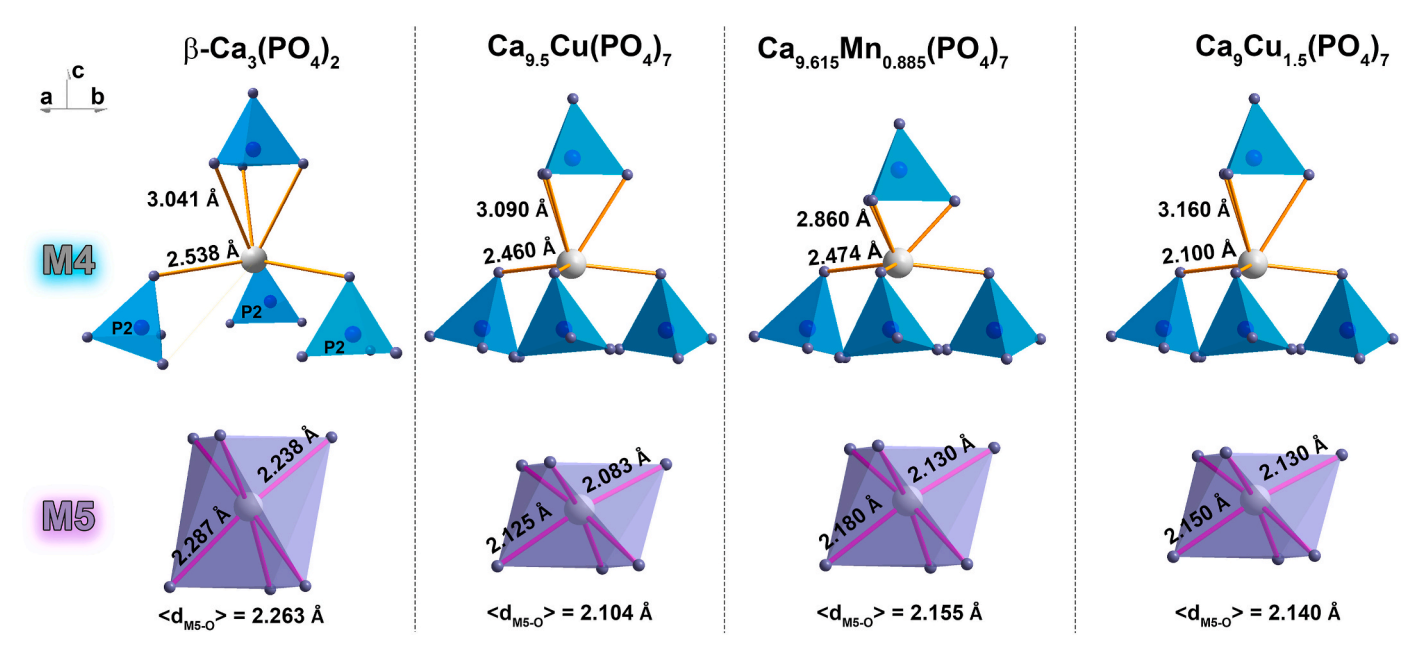


Fig. 8. Polyhedra of M4 and M5 sites in the β -Ca₃(PO₄)₂-type structures.

the M3 site and less amounts will be located in the M1 and M2 sites. The M4 site is half-occupied by Sr^{2+} . In the case of strontium and copper co-doping in the β -Ca₃(PO₄)₂ structure, it was shown that Cu^{2+} cations are located in the M5 sites, and Sr^{2+} cations occupy the M4 sites [19].

The incorporation of Sr^{2+} ions along with the divalent metal ions allows to extend the existence limit of a solid solution due to the enlargement of the unit cell. The unit cell parameters and volume of codoped compounds directly depend on the radii of the incorporated ions.

In Sr^{2+}/Mn^{2+} and Sr^{2+}/Cu^{2+} samples the single-phase compounds were observed at x=0.25 in $Ca_{3-2x}(SrM')_x(PO_4)_2$, $M'=Mn^{2+}$ or Cu^{2+} according to occupation of the different M4 and M5 sites in the structure by Sr^{2+} and M', respectively. According to the previous data [19,49–51] Sr^{2+} ions are located in M1–M4 sites in β -TCP. Moreover, with an increase in the Sr^{2+} concentration, the M4 sites are firstly populated (half-occupied), followed by the M1, M2 and M3 sites by Sr^{2+} . The crystal chemical formula of β -TCP-Cu+Sr ($Ca_{2.5}Cu_{0.25}Sr_{0.25}(PO_4)_2$ Z =

21) can be shown as $Ca(1,2,3)_{8.625}Sr(1,2,3)_{0.375}Sr(4)_{0.5}Cu_{0.875}(5)C$ $a_{0.125}(5)(PO_4)_7$ (Z = 6). Thus, in β -TCP-Cu+Sr the strontium ions are placed as $2.25Sr^{2+}$ (in each M1, M2, M3 sites) and $3Sr^{2+}$ (M4 sites), respectively. The occupancy (a_i) of M5 is $a_i = 5.25Cu^{2+} + 0.75Ca^{2+}$. So, the absence of competition in the location in the crystal structure allows to incorporate higher concentrations of active antibacterial Cu^{2+} ions.

It can be concluded that the Cu^{2+} cations location (M5 or M4 sites) depends on the treatment conditions and concentration of Cu^{2+} ions. The location of Sr^{2+} cations (M1, M2, M3 and M4) depends only on its concentration. The Zn^{2+} and Mn^{2+} cations in the studied compounds can occupy solely the M5 site. Earlier, structural factors and the preparation conditions of doped and co-doped phases with the β - $Ca_3(PO_4)_2$ -type structure were not taken into account during the antibacterial activity studies [33,34,38,44,49].

In the case of co-doping samples with small divalent ions, such as Zn^{2+} , Mg^{2+} , Cu^{2+} , Mn^{2+} , these ions are competing in the occupation of the octahedral M5 site, and the excess of the doping ions forms the impurities. This fact is responsible for the appearance of the impurity $Zn_3(PO_4)_2$ phase in Zn^{2+}/Cu^{2+} co-doped sample β -TCP-Cu-Zn.

The combination (location) of two different ions in the M5 and M1, M2, M3 and M4 sites significantly booster the antibacterial properties. This is confirmed by the fact that the single-doped β -TCP-Cu sample exhibits one of the smallest inhibition activities among the investigated phosphates. The inhibition activity reaches 56.5% for *C. albicans*, while it was only 27.7% for *E. coli*.

The co-doped phosphates exhibit enhanced antimicrobial properties with respect to the various microorganisms. The minimal growth of the bacteria and fungus was observed in all experiments using β -TCP-Cu+Sr. It should also be noted that this composition is single-phase, and the concentration of Cu²⁺ was the highest among co-doped samples. The increasing of antimicrobial activity in β -TCP-Cu+Sr is related to the incorporation of Sr²⁺ and stimulation of Cu²⁺ ions. It follows from the above analysis that substitution by Sr²⁺ into the M1–M4 positions noticeably affects antimicrobial activity. In addition, the combination of ions in the M5 and M1–M4 sites also has a significant effect on antimicrobial properties. The combination (location) of Cu²⁺+Sr²⁺ ions in the structure provides the highest antimicrobial activity. The inhibition rate of β -TCP-Cu+Sr reaches 92.0, 95.5, 64.9, 96.3, 70.9% on *S. aureus*, *P. aeruginosa*, *E. coli*, *E. faecalis* and *C. albicans*, respectively.

The other phosphates show the selective character of their efficacy against individual microorganisms. Since the Zn^{2+} and Cu^{2+} ions are located in the same M5 sites in β -TCP their different antimicrobial activity apparently is related to their electronic structure. The best results were obtained for *P. aeruginosa* and *E. faecalis* with the inhibition rate at 79.3% and 77.4%, respectively. Therefore, these results confirm the assumption that active dopant ions must be located in different crystal sites for providing higher antimicrobial activity. So, β -TCP-Cu+Sr inhibits bacterial growth better than β -TCP-Cu+Zn.

The composition β -TCP-Mn+Sr shows the least efficiently against microorganisms. The co-substitution by Mn²⁺+Sr²⁺ ions into the β -TCP structure is accompanied by the appearance of the lowest antibacterial activity (excluding the bacterium *P. aeruginosa*) and reaches only 19.0%, 41.9% and 57.8% on *E. coli, C. albicans* and *S. aureus*, respectively. The absence of significant antibacterial activity was previously observed in Mn²⁺-doped TCP compounds [26], however it can promote cell viability [52] and pre-osteoblastic proliferation and differentiation [53].

The antimicrobial activity of the ions is probably due to damage to the cytoplasmic membrane, the denaturation of proteins and damage to the DNA of the microorganisms. The exact mechanism of the activity of metal ions is still unknown, but the simultaneous presence of different ions generally increases antimicrobial activity due to the combination of actions. In fact, as evidenced by the experiments, the association of different ions had a stronger effect on the inhibition of the growth of microorganisms rather than single ions.

5. Conclusions

The substituted Ca^{2+}/Cu^{2+} , and co-substituted Cu^{2+}/Zn^{2+} , Cu^{2+}/Sr^{2+} , and Sr^{2+}/Mn^{2+} β -TCP-based phosphates have been synthesized and their antibacterial properties were studied. The X-ray diffraction studies show the formation of β -TCP-type structure as the main phase. The analysis of the chemical compositions in correlation with the structural features of the β -TCP structure has been done. It has been established that single phase $Ca_{3\cdot 2x}(M'M'')_x(PO_4)_2$ solid solutions can be formed only at $x \leq 0.286$, where M' and M'' – divalent metal ions, such as Zn^{2+} , Mg^{2+} , Cu^{2+} , Mn^{2+} , etc. The incorporation of Sr^{2+} ions along with the divalent metal ions allows to extend the existence limit of a solid solution due to the enlargement of the unit cell.

It was shown that all synthesized phases have an antibacterial effect. The minimal growth of the bacteria and fungus was observed in all experiments using $\beta\text{-TCP-Cu+Sr}$ with the highest concentration of Cu^{2+} ions among all studied samples and separate occupation of crystal sites. The phosphates with joint occupation of M5 site show the selective character of their efficacy against individual microorganisms. So, the active dopant ions must be located in different crystal sites for providing higher antimicrobial activity.

Declaration of competing interest

The authors declare that they have no known competing financial interests or personal relationships that could have appeared to influence the work reported in this paper.

Acknowledgements

The work was partially supported by the bilateral project CNR (Italy) - NSFC (China) 2021–2022. I.F.V. is grateful for financial support of the Russian Science Foundation (Project No. 22-23-00278). The technical support of Mr. Marco Ortenzi, Mr. Massimo Di Menno Di Bucchianico and Mr. Luca Imperatori is gratefully acknowledged. The X-ray study was carried out in accordance with the state of the Russian Federation, state registration number 122011300125-2.

References

- [1] R. Gopal, C. Calvo, J. Ito, W.K. Sabine, Crystal structure of synthetic Mg-whitlockite, $Ca_{18}Mg_2H_2(PO_4)_{14}$, Can. J. Chem. 52 (1974) 1155–1164, https://doi.org/10.1139/v74-181.
- [2] G. Kazakova, T. Safronova, D. Golubchikov, O. Shevtsova, J.V. Rau, Resorbable Mg²⁺-containing phosphates for bone tissue repair, Materials 14 (2021) 4857, https://doi.org/10.3390/ma14174857.
- [3] D.V. Deyneko, S.M. Aksenov, V.A. Morozov, S.Y. Stefanovich, O.V. Dimitrova, O. V. Barishnikova, B.I. Lazoryak, A new hydrogen-containing whitlockitetype phosphate Ca₉(Fe_{0.63}Mg_{0.37})H_{0.37}(PO₄)₇: hydrothermal synthesis and structure, Zeitschrift Fur Krist. Cryst. Mater. 229 (2014), https://doi.org/10.1515/zkri-2014.1774
- [4] E. Boanini, M. Gazzano, C. Nervi, M.R. Chierotti, K. Rubini, R. Gobetto, A. Bigi, Strontium and zinc substitution in β-tricalcium phosphate: an X-ray diffraction, solid state NMR and ATR-FTIR study, J. Funct. Biomater. 10 (2019), https://doi. org/10.3390/jfb10020020.
- [5] A. Altomare, R. Rizzi, M. Rossi, A. El Khouri, M. Elaatmani, V. Paterlini, G. Della Ventura, F. Capitelli, New $Ca_{2.90}(Me^{2+})_{0.10}(PO_4)_2$ β -tricalcium phosphates with $Me^{2+}=Mn$, Ni, Cu: synthesis, crystal-chemistry, and luminescence properties, Crystals 9 (2019) 288, https://doi.org/10.3390/cryst9060288.
- [6] I.V. Fadeeva, D.V. Deyneko, K. Barbaro, G.A. Davydova, M.A. Sadovnikova, F. F. Murzakhanov, A.S. Fomin, V.G. Yankova, I.V. Antoniac, S.M. Barinov, B. I. Lazoryak, J.V. Rau, Influence of synthesis conditions on gadolinium-substituted tricalcium phosphate ceramics and its physicochemical, biological, and antibacterial properties, Nanomaterials 12 (2022) 852, https://doi.org/10.3390/nano12050852.
- [7] E. Bonnelye, A. Chabadel, F. Saltel, P. Jurdic, Dual effect of strontium ranelate: stimulation of osteoblast differentiation and inhibition of osteoclast formation and resorption in vitro, Bone 42 (2008) 129–138, https://doi.org/10.1016/j. bone 2007 08 043
- [8] Y. Yamada, A. Ito, H. Kojima, M. Sakane, S. Miyakawa, T. Uemura, R.Z. LeGeros, Inhibitory effect of Zn²⁺ in zinc-containing β-tricalcium phosphate on resorbing activity of mature osteoclasts, J. Biomed. Mater. Res., Part A 84A (2008) 344–352, https://doi.org/10.1002/jbm.a.31265.

- [9] F. Salamanna, G. Giavaresi, D. Contartese, A. Bigi, E. Boanini, A. Parrilli, R. Lolli, A. Gasbarrini, G. Barbanti Brodano, M. Fini, Effect of strontium substituted β-TCP associated to mesenchymal stem cells from bone marrow and adipose tissue on spinal fusion in healthy and ovariectomized rat, J. Cell. Physiol. 234 (2019) 20046–20056, https://doi.org/10.1002/jcp.28601.
- [10] K. Spaeth, F. Goetz-Neunhoeffer, K. Hurle, Cu²⁺ doped β-tricalcium phosphate: solid solution limit and crystallographic characterization by rietveld refinement, J. Solid State Chem. 285 (2020), 121225, https://doi.org/10.1016/j.issc.2020.121225.
- [11] I.V. Fadeeva, M.R. Gafurov, I.A. Kiiaeva, S.B. Orlinskii, L.M. Kuznetsova, Y. Y. Filippov, A.S. Fomin, G.A. Davydova, I.I. Selezneva, S.M. Barinov, Tricalcium phosphate ceramics doped with silver, copper, zinc, and iron (III) ions in concentrations of less than 0.5 wt.% for bone tissue regeneration, Bionanoscience 7 (2017) 434–438, https://doi.org/10.1007/s12668-016-0386-7.
- [12] I.V. Fadeeva, B.I. Lazoryak, G.A. Davidova, F.F. Murzakhanov, B.F. Gabbasov, N. V. Petrakova, M. Fosca, S.M. Barinov, G. Vadalà, V. Uskoković, Y. Zheng, J.V. Rau, Antibacterial and cell-friendly copper-substituted tricalcium phosphate ceramics for biomedical implant applications, Mater. Sci. Eng., C 129 (2021), 112410, https://doi.org/10.1016/j.msec.2021.112410.
- [13] E. Boanini, P. Torricelli, F. Sima, E. Axente, M. Fini, I.N. Mihailescu, A. Bigi, Gradient coatings of strontium hydroxyapatite/zinc β-tricalcium phosphate as a tool to modulate osteoblast/osteoclast response, J. Inorg. Biochem. 183 (2018) 1–8, https://doi.org/10.1016/j.jinorgbio.2018.02.024.
- [14] S. Samani, S.M. Hossainalipour, M. Tamizifar, H.R. Rezaie, In vitro antibacterial evaluation of sol-gel-derived Zn-, Ag-, and (Zn+Ag)-doped hydroxyapatite coatings against methicillin-resistant Staphylococcus aureus, J. Biomed. Mater. Res., Part A 101A (2013) 222–230, https://doi.org/10.1002/jbm.a.34322.
- [15] M. Roy, S. Bose, Osteoclastogenesis and osteoclastic resorption of tricalcium phosphate: effect of strontium and magnesium doping, J. Biomed. Mater. Res., Part A (2012), https://doi.org/10.1002/jbm.a.34181 n/a-n/a.
- [16] J. Wang, J. Qian, W. Xu, Y. Wang, G. Hou, T. Sun, L. Luo, Effects of Sr²⁺/Zn²⁺ co-substitution on crystal structure and properties of nano-β-tricalcium phosphate, Ceram. Int. 44 (2018) 6096–6103, https://doi.org/10.1016/j.ceramint.2017.12.242.
- [17] M. Roy, G.A. Fielding, A. Bandyopadhyay, S. Bose, Effects of zinc and strontium substitution in tricalcium phosphate on osteoclast differentiation and resorption, Biomater. Sci. 1 (2013) 74–82, https://doi.org/10.1039/c2bm00012a.
- [18] N. Somers, F. Jean, M. Lasgorceix, H. Curto, G. Urruth, A. Thuault, F. Petit, A. Leriche, Influence of dopants on thermal stability and densification of β-tricalcium phosphate powders, Open Ceram. 7 (2021), 100168, https://doi.org/ 10.1016/j.oceram.2021.100168.
- [19] P.N. Kumar, M. Boovarasan, R.K. Singh, S. Kannan, Synthesis, structural analysis and fabrication of coatings of the Cu^{2+} and Sr^{2+} co-substitutions in β -Ca₃(PO₄)₂, RSC Adv. 3 (2013) 22469–22479, https://doi.org/10.1039/c3ra43171a.
- [20] R.K. Singh, S. Kannan, Synthesis, Structural analysis, Mechanical, antibacterial and Hemolytic activity of Mg²⁺ and Cu²⁺ co-substitutions in β-Ca₃(PO₄)₂, Mater. Sci. Eng., C 45 (2014) 530–538, https://doi.org/10.1016/j.msec.2014.10.017.
- [21] D.F. Macedo, A.F. Cunha, J.F. Mano, M.B. Oliveira, A.P. Silva, Tricalcium phosphate doped with Mg²⁺ and combinations of Mn²⁺, Zn²⁺ and Fe³⁺: a DoE study on sintering, mechanical, microstructural and biological properties, Ceram. Int. (2022), https://doi.org/10.1016/j.ceramint.2022.04.004.
- [22] L. Sinusaite, A. Popov, A. Antuzevics, K. Mazeika, D. Baltrunas, J.-C. Yang, J. L. Horng, S. Shi, T. Sekino, K. Ishikawa, A. Kareiva, A. Zarkov, Fe and Zn cosubstituted beta-tricalcium phosphate (β-TCP): synthesis, structural, magnetic, mechanical and biological properties, Mater. Sci. Eng., C 112 (2020), 110918, https://doi.org/10.1016/j.msec.2020.110918.
- [23] Y.-J. Chou, H.S. Ningsih, S.-J. Shih, Preparation, characterization and investigation of antibacterial silver-zinc co-doped β-tricalcium phosphate by spray pyrolysis, Ceram. Int. 46 (2020) 16708–16715, https://doi.org/10.1016/j. ceramint 2020 03 245
- [24] N. Matsumoto, K. Sato, K. Yoshida, K. Hashimoto, Y. Toda, Preparation and characterization of β-tricalcium phosphate co-doped with monovalent and divalent antibacterial metal ions, Acta Biomater. 5 (2009) 3157–3164, https://doi.org/ 10.1016/j.actbio.2009.04.010.
- [25] R. Meenambal, P. Nandha Kumar, P. Poojar, S. Geethanath, S. Kannan, Simultaneous substitutions of Gd³⁺ and Dy³⁺ in β-Ca₃(PO₄)₂ as a potential multifunctional bio-probe, Mater. Des. 120 (2017) 336–344, https://doi.org/ 10.1016/j.matdes.2017.02.013.
- [26] T. Ates, S.V. Dorozhkin, O. Kaygili, M. Kom, I. Ercan, N. Bulut, F. Firdolas, S. Keser, N.C. Gursoy, I.H. Ozercan, Y. Eroksuz, T. İnce, The effects of Mn and/or Ni dopants on the in vitro/in vivo performance, structural and magnetic properties of β-tricalcium phosphate bioceramics, Ceram. Int. 45 (2019) 22752–22758, https://doi.org/10.1016/j.ceramint.2019.07.314.
- [27] R.K. Singh, M. Srivastava, N.K. Prasad, S. Kannan, Structural Analysis and Hyperthermia Effect of Fe³⁺/Ni²⁺ Co-substitutions in β-Ca₃(PO₄)₂, Elsevier B.V., 2017, https://doi.org/10.1016/j.jallcom.2017.07.113.
- [28] R.K. Singh, M. Srivastava, N.K. Prasad, P.H. Shetty, S. Kannan, Hyperthermia effect and antibacterial efficacy of Fe³⁺/Co²⁺ co-substitutions in β-Ca₃(PO₄)₂ for bone cancer and defect therapy, J. Biomed. Mater. Res. Part B Appl. Biomater. 106 (2018) 1317–1328, https://doi.org/10.1002/jbm.b.33921.
- [29] R. Singh, M. Srivastava, N.K. Prasad, S. Awasthi, A. Kumar Dhayalan, S. Kannan, Structural analysis and magnetic induced hyperthermia of Fe³⁺ and Mn²⁺

- substituted β -Ca₃(PO₄)₂, New J. Chem. 41 (2017) 12879–12891, https://doi.org/ 10.1039/c7ni01228d.
- [30] V. Petricek, M. Dusek, L. Palatinus, V. Petrícek, M. Dušek, L. Palatinus, Crystallographic computing system JANA2006: general features, Zeitschrift Fur Krist 229 (2014) 345–352, https://doi.org/10.1515/zkri-2014-1737.
- [31] B. Dickens, L.W. Schroeder, W.E. Brown, Crystallographic studies of the role of Mg as a stabilizing impurity in β-Ca₃(PO₄)₂. The crystal structure of pure β-Ca₃(PO₄)₂, J. Solid State Chem. 10 (1974) 232–248, https://doi.org/10.1016/0022-4596(74) 90030-9.
- [32] R.J.B. Jakeman, A.K. Cheetham, N.J. Clayden, C.M. Dobson, Phosphorus-31 magic angle spinning NMR study of the cation distribution in Zn_{3-x}Mg_x(PO₄)₂, J. Am. Chem. Soc. 107 (1985) 6249–6252, https://doi.org/10.1021/ja00308a017.
- [33] A.A. Belik, O.V. Yanov, B.I. Lazoryak, Synthesis and crystal structure of Ca₉Cu_{1.5}(PO₄)₇ and reinvestigation of Ca_{9.5}Cu(PO₄)₇, Mater. Res. Bull. 36 (2001) 1863–1871, https://doi.org/10.1016/S0025-5408(01)00666-3.
- [34] A.A. Belik, F. Izumi, S.Y. Stefanovich, A.P. Malakho, B.I. Lazoryak, I.A. Leonidov, O.N. Leonidova, S.A. Davydov, Polar and centrosymmetric phases in solid solutions Ca_{3-x}Sr_x(PO₄)₂ (0 ≤ x ≤ 16/7), Chem. Mater. 14 (2002) 3197–3205, https://doi. org/10.1021/cm0202431.
- [35] M. Yashima, A. Sakai, T. Kamiyama, A. Hoshikawa, Crystal structure analysis of β-tricalcium phosphate Ca₃(PO₄)₂ by neutron powder diffraction, J. Solid State Chem. 175 (2003) 272–277, https://doi.org/10.1016/S0022-4596(03)00279-2.
- [36] R.D. Shannon, Revised effective ionic radii and systematic studies of interatomic distances in halides and chalcogenides, Acta Crystallogr. A 32 (1976) 751–767, https://doi.org/10.1107/S0567739476001551.
- [37] B.C. Cornilsen, R.A. Condrate, The vibrational spectra of β -Ca₂P₂O₇ and γ -Ca₂P₂O₇, J. Inorg. Nucl. Chem. 41 (1979) 602–605, https://doi.org/10.1016/0022-1902(79) 80457-1.
- [38] N. Khan, V.A. Morozov, S.S. Khasanov, B.I. Lazoryak, Synthesis and crystal structure of calcium copper phosphate, s-Ca₁₉Cu₂(PO₄)₁₄, Mater. Res. Bull. 32 (1997) 1211–1220, https://doi.org/10.1016/S0025-5408(97)00098-6.
- [39] A. Bessière, A. Lecointre, R.A. Benhamou, E. Suard, G. Wallez, B. Viana, How to induce red persistent luminescence in biocompatible Ca₃(PO₄)₂, J. Mater. Chem. C 1 (2013) 1252–1259, https://doi.org/10.1039/C2TC00138A.
- [40] A. Benarafa, M. Kacimi, G. Coudurier, M. Ziyad, Characterisation of the active sites in butan-2-ol dehydrogenation over calcium–copper and calcium–sodium–copper phosphates, Appl. Catal. Gen. 196 (2000) 25–35, https://doi.org/10.1016/S0926-860X(99)00446-9.
- [41] A.G. Nord, Incorporation of divalent metals in whitlockite-related β -Ca₃(PO₄)₂, N. Jb. Miner. Mh. 11 (1983) 489.
- [42] S.S. Romdhane, G. Bonel, G. Bacquet, Localisation par résonance paramagnétique electronique de l'impureté cuivre dans le phosphate tricalcique β, Mater. Res. Bull. 18 (1983) 559–568, https://doi.org/10.1016/0025-5408(83)90213-1.
- [43] B.I. Lazoryak, N. Khan, V.A. Morozov, A.A. Belik, S.S. Khasanov, Preparation, structure determination, and redox characteristics of new calcium copper phosphates, J. Solid State Chem. 145 (1999) 345–355, https://doi.org/10.1006/ jssc.1999.8294.
- [44] O.V. Yanov, V.A. Morozov, B.N. Vieting, L.N. Ivanov, B.I. Lazoryak, A whitlockite-like calcium copper phosphate, Mater. Res. Bull. 29 (1994) 1307–1314, https://doi.org/10.1016/0025-5408(94)90155-4.
- [45] G. Zhu, Z. Ci, Y. Shi, M. Que, Q. Wang, Y. Wang, Synthesis, crystal structure and luminescence characteristics of a novel red phosphor Ca₁₉Mg₂(PO₄)₁₄:Eu³⁺ for light emitting diodes and field emission displays, J. Mater. Chem. C 1 (2013) 5960–5969, https://doi.org/10.1039/c3tc31263a.
- [46] E. Kreidler, Phase equilibria in the system $Ca_3(PO_4)_2$ - $Zn_3(PO_4)_2$, Inorg. Chem. 6 (1967) 524–528.
- [47] L. Carbajal, M.A. Sainz, S. Serena, A.C. Caballero, Á. Caballero, Solid-state compatibility in two regions of the system ZnO-CaO-P₂O₅, J. Am. Ceram. Soc. 94 (2011) 2213–2219, https://doi.org/10.1111/j.1551-2916.2010.04355.x.
- [48] A. Lecointre, R. Ait Benhamou, A. Bessiére, G. Wallez, M. Elaatmani, B. Viana, Red long-lasting phosphorescence (LLP) in β-TCP type Ca_{9.5}Mn(PO₄)₇compounds, in: Opt. Mater., Amst)., 2011, https://doi.org/10.1016/j.optmat.2011.05.020.
- [49] H. Ji, Z. Huang, Z. Xia, M.S. Molokeev, V.V. Atuchin, M. Fang, S. Huang, New yellow-emitting whitlockite-type structure Sr_{1.75}Ca_{1.25}(PO₄)₂:Eu²⁺ phosphor for near-UV pumped white light-emitting devices, Inorg. Chem. 53 (2014) 5129–5135, https://doi.org/10.1021/ic500230v.
- [50] G. Renaudin, P. Laquerrière, Y. Filinchuk, E. Jallot, J.M. Nedelec, Structural characterization of sol-gel derived Sr-substituted calcium phosphates with antiosteoporotic and anti-inflammatory properties, J. Mater. Chem. 18 (2008) 3593, https://doi.org/10.1039/b804140g.
- [51] S.Y. Stefanovich, D.A. Petrova, V.A. Morozov, E.A. Fortalnova, D.A. Belov, D. V. Deyneko, B.I. Lazoryak, Enhanced nonlinear optical activity and Ca²⁺-conductivity in Ca_{10.5-x}Pb_x(VO₄)₇ ferroelectrics, J. Alloys Compd. 735 (2018) 1826–1837, https://doi.org/10.1016/j.jallcom.2017.11.172.
- [52] L. Sinusaite, A.M. Renner, M.B. Schütz, A. Antuzevics, U. Rogulis, I. Grigoraviciute-Puroniene, S. Mathur, A. Zarkov, Effect of Mn doping on the low-temperature synthesis of tricalcium phosphate (TCP) polymorphs, J. Eur. Ceram. Soc. 39 (2019) 3257–3263, https://doi.org/10.1016/j.jeurceramsoc.2019.03.057.
- [53] P.M.C. Torres, S.I. Vieira, A.R. Cerqueira, S. Pina, O.A.B. Da Cruz Silva, J.C. C. Abrantes, J.M.F. Ferreira, Effects of Mn-doping on the structure and biological properties of β-tricalcium phosphate, J. Inorg. Biochem. 136 (2014) 57–66, https://doi.org/10.1016/j.jinorgbio.2014.03.013.